Article:

Malmierca-Vallet, I, Sime, LC, Tindall, JC et al. (4 more authors) (2018) Simulating the Last Interglacial Greenland stable water isotope peak: The role of Arctic sea ice changes. Quaternary Science Reviews, 198. pp. 1-14. ISSN 0277-3791

https://doi.org/10.1016/j.quascirev.2018.07.027

Simulating the Last Interglacial Greenland stable water isotope peak: the role of Arctic sea ice changes

Irene Malmierca-Vallet [a, b], Louise C. Sime [a], Julia C. Tindall [c], Emilie Capron [a, d], Paul J. Valdes [b], Bo M. Vinther [d], Max D. Holloway [a]

[a] British Antarctic Survey, High Cross, Madingley Road, Cambridge, CB3 0ET, UK

[b] School of Geographical Sciences, University of Bristol, University Road, Bristol, BS8 1SS, UK

[c] School of Earth and Environment, University of Leeds, Leeds, LS2 9JT, UK

[d] Centre for Ice and Climate, Niels Bohr Institute, University of Copenhagen, Juliane Maries Vej 30, DK-2900, Copenhagen, Denmark

Abstract

Last Interglacial (LIG), stable water isotope values ($\delta^{18}O$) measured in Greenland deep ice cores are at least 2.5‰ higher compared to the present day. Previous isotopic climate simulations of the LIG do not capture the observed Greenland $\delta^{18}O$ increases. Here, we use the isotope-enabled HadCM3 (UK Met Office coupled atmosphere-ocean general circulation model) to investigate whether a retreat of Northern Hemisphere sea ice was responsible for this model-data disagreement. Our results highlight the potential significance of sea ice changes on the LIG Greenland isotopic maximum. Sea ice loss in combination with increased sea surface temperatures, over the Arctic, affect $\delta^{18}O$: water vapour enriched in heavy isotopes and a shorter distillation path may both increase $\delta^{18}O$ values over Greenland. We show, for the first time, that simulations of the response to Arctic sea ice reduction are capable of producing the likely magnitude of LIG $\delta^{18}O$ increases at NEEM, NGRIP, GIPS2 and Camp Century ice core sites. However, we may underestimate $\delta^{18}O$ changes at the Renland, DYE3 and GRIP ice core locations. Accounting for possible ice sheet changes is likely to be required to produce a better fit to the ice core measurements.

1. <u>Introduction</u>

Polar Regions are especially sensitive to variations in radiative forcing; they can act as amplifiers of climate change via albedo feedbacks (e.g. Vaughan et al., 2013). Studying these climate feedback processes is fundamental for better understanding future high-latitude responses to increasing greenhouse gas (GHG) emissions. Past warm periods like the Last Interglacial (LIG, approximately 129 - 116 thousand of years BP, hereafter ka) provide an ideal case study to evaluate the capability of climate models to appropriately capture processes involved in polar amplification (e.g. Otto-Bliesner et al., 2013; Schmidt et al., 2014).

During the LIG, large parts of the Earth showed warmer conditions compared to present day (e.g. CAPE Last Interglacial Project Members, 2006; Turney and Jones, 2010). The increase in summertime insolation at northern high latitudes contributed to a warmer-than-present-day Arctic region (CAPE Last Interglacial Project Members, 2006; Masson- Delmotte et al., 2013), and maximum global sea level reached 6 to 9 m above present level (e.g. Dutton et al., 2015; Kopp et al., 2009).

Little is known about the precise extent or concentration of Northern Hemisphere (NH) sea ice during the LIG. Figure 1 and supplementary table 1 show the sparse set of available observations of NH sea ice changes for the LIG. As recent data compilations show that high northern latitude surface air temperatures (SATs) and sea surface temperatures (SSTs) were warmer in the LIG (Capron et al., 2014, 2017; Hoffman et al., 2017), it is probable that there was both reduced winter and summer sea ice extent compared to today. This is supported by marine cores located in the Arctic Ocean (figure 1 : GreenICE and HLY0503-8JPC cores) which show planktonic foraminifers characteristic of subpolar, seasonally open waters were present at these sites during the LIG, possibly reflecting ice free summer conditions in the central LIG Arctic Ocean.

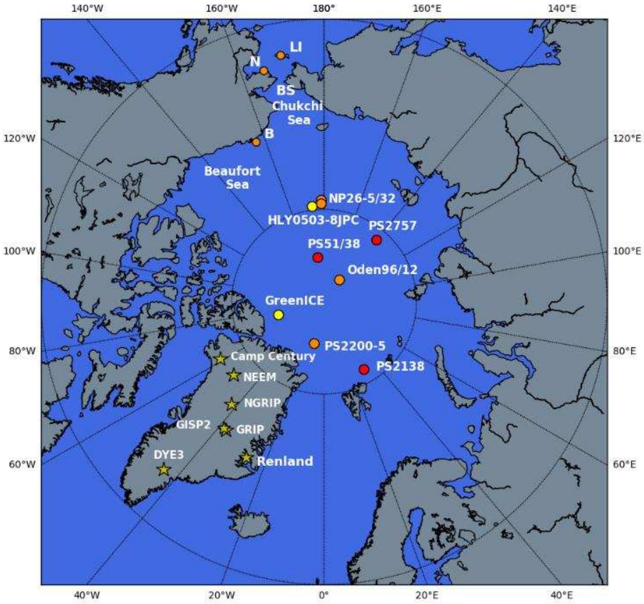

Figure 1. Map of the Arctic Ocean showing the position of observations of sea ice change based on subpolar foraminifers (yellow circles), mollusc and ostracode faunas (orange circles) and biomarker proxy IP25 (red circles). Also indicated are key regions: St Lawrence Island (LI), Nome (N), Bering Strait (BS), Barrow (B). Also shown are Greenland ice cores (yellow stars) which contain LIG ice: NEEM (77.5°N, 51.1°W), NGRIP (75.1°N, 42.3°W), GRIP (72.6°N, 37.6°W), GISP2 (72.6°N, 38.5°W), Renland (71.3°N, 26.7°W), DYE3 (65.2°N, 43.8°W) and Camp Century (77.2°N 61.1°W).

In addition, LIG deposits on the Chukchi Sea coast include fossils of species presently known to be limited to the warmer northwest Pacific, while intertidal snails retrieved close to Nome suggest annually ice-free conditions around the coast south of the currently seasonally ice covered Bering Strait (Brigham-Grette and Hopkins, 1995; Brigham-Grette et al., 2001). Deposits close to Barrow contain some ostracode species that are only found today in the North Atlantic and deposits on the Alaskan Coastal Plain indicate that several mollusc species expanded their range well into the Beaufort Sea (Brigham-Grette and Hopkins, 1995). The nature of marine faunas at St. Lawrence Island, Beaufort Sea shelf and Nome suggests that winter sea ice did not expand south of Bering Strait, and that the Bering Sea was annually ice-free (Brigham-Grette and Hopkins, 1995) (figure 1 and supplementary table 1). Additionally, the ostracode sea ice proxy of Cronin et al. (2010) (figure 1 : NP26-5/32, Oden96/12-1pc and PS2200-5 cores) agree with the idea of sea ice glacial-interglacial variability, with sea-ice maximum on the Morris Jesup Rise and the Lomonosov and Mendeleyev Ridges during interglacial-to-glacial transitions and minimum coverage during peak interglacial periods (e.g. MIS 5e) (supplementary table 1).

In a recent study, a more direct sea ice proxy named “IP25” is used in combination with terrestrial and open-water phytoplankton biomarkers to reconstruct the Arctic sea ice distribution during the LIG (Stein et al., 2017). The authors propose relatively closed sea ice cover conditions over PS2757-8 core (figure 1 and supplementary table 1), possibly ice-free conditions in the direction of the East Siberian shelf and significantly reduced sea ice cover over the Barents Sea continental margin (figure 1: PS2138-2 core). In contrast to previous studies (e.g. Adler et al. 2009), that point to an Arctic Ocean perhaps free of summer sea ice, Stein et al. (2017) indicate the presence of perennial sea ice in two cores from central Arctic Ocean during MIS 5e (figure 1: PS2200-5 and PS51/038-3 cores). Note, however, planktonic foraminifers were also present at these two sites (PS2200-5 and PS51/038-3) during the LIG, possibly reflecting phases of summer open-water conditions to allow foraminifers to reproduce (Spielhagen et al., 2004).

Measurements of stable water isotopes, $\delta^{18}O$ and δD, in ice cores yield useful information on past temperature changes. High-latitude local temperature is a principal control on the distribution of $\delta^{18}O$ and δD in preserved Greenland ice (Dansgaard, 1964). Originally, $\delta^{18}O$ measurements have been translated into temperature making use of a linear relationship ($\delta^{18}O = aT+b$, T being surface temperature) obtained from spatial information (e.g Dansgaard, 1964; Jouzel et al., 1994, 1997). However, over the last decades, it has become evident that this isotope-temperature relationship is affected by atmospheric transport, evaporation conditions and precipitation intermittency, and therefore varies in both space and time (e.g. Jouzel et al., 1997; Masson-Delmotte et al., 2011). By influencing these key aspects, sea ice condition changes have been proposed to exert significant control over the distribution of isotopes in polar ice (e.g. Holloway et al., 2016a; Holloway et al., 2017; Rehfeld et al., 2018; Sime et al., 2013).

LIG ice layers have been found in numerous Greenland deep ice cores (figure 1) (e.g. NGRIP Project Members, 2004; NEEM community members, 2013; Landais et al., 2016 for a review). The LIG $\delta^{18}O$ anomaly estimated at the initial snowfall NEEM deposition site (value of 3.6‰ at 126 ka) was translated into precipitation-weighted surface temperatures 7.5 ±1.8°C warmer compared to the last millennium and +8±4°C when accounting for Greenland ice sheet elevation changes and upstream effects (NEEM community members, 2013). LIG climate simulations in response to GHG and orbital forcing alone fail to capture these anomalies for both $\delta^{18}O$ and temperature (e.g. Lunt et al., 2013; Masson-Delmotte et al., 2013; Otto-Bliesner et al., 2013; Sjolte et al., 2014). Recent sensitivity studies show that changes in the GIS topography and sea ice retreat in the Nordic Seas can lead to enhanced surface warming (up to 5°C) in northwest Greenland, reducing the mismatch between models and data (Merz et al., 2014a, 2016).

Whereas the temperature profile measured in the borehole can be used to calibrate the Holocene isotope-temperature slope (Vinther et al., 2009), this is not possible for the LIG as palaeotemperatures for this period are not conserved in the ice sheet. This means that, the use of isotopically enabled General Circulation Models (GCMs) is probably the best available method to constrain the LIG isotope-temperature slope (e.g. Sime et al., 2013; Sjolte et al., 2014). Previous isotopic climate simulations of the LIG underestimate the $\delta^{18}O$ anomalies of ~ +3‰ observed in Greenland ice cores (Masson-Delmotte et al., 2011; Sjolte et al., 2014). An exception is the study carried out by Sime et al. (2013) where Greenland $\delta^{18}O$ anomalies of >3‰ are simulated over central Greenland. Note, however, that Sime et al. (2013) use GHG-forced simulations as analogies for the LIG climate which could be problematic because the climate response to the anthropogenic forcing projected for the near future is essentially different from the climate response to the orbital forcing characteristic of the LIG warmth.

Here we therefore aim to better understand the processes behind the LIG Greenland isotope peak. In particular, we investigate whether a retreat of NH sea ice could have been responsible for the Greenland isotopic maximum. Thus, we design a set of LIG sea ice sensitivity experiments that complement previous modelling studies with the detailed investigation of the role of NH sea ice changes on LIG isotopic simulations.

In overview, we first describe the isotopic model and explain the design of the LIG sea ice sensitivity experiments. Secondly, we compile LIG Greenland isotopic as well as Arctic and Atlantic sea surface observations. Third, we analyse the modelled NH anomalies for $\delta^{18}O$ and temperature and discuss the response of the hydrological cycle to sea ice retreat. Finally, we summarise our findings and draw together some conclusions.

2. <u>Methods</u>

2.1. <u>Model description</u>

In order to investigate the isotopic response to a retreat of NH sea ice, we use the isotope-enabled HadCM3 (Hadley Centre Coupled Model Version 3); a UK Met Office coupled atmosphere-ocean GCM. The horizontal grid spacing of the atmosphere component is 2.5° (latitude) by 3.75° (longitude) with 19 vertical levels (Gordon et al., 2000). The ocean component has a horizontal grid resolution of 1.25° by 1.25° and has 20 vertical levels (Gordon et al., 2000). In addition to the ocean and atmosphere components, HadCM3 also includes sea ice and vegetation components (Gordon et al., 2000). We use the TRIFFID (Top-down Representation of Interactive Foliage and Flora Including Dynamics) dynamic global vegetation model and the MOSES 2.1 land surface scheme where energy and water fluxes between the surface and the atmosphere are calculated.

HadCM3 has been used to investigate the Last Glacial Maximum (Holloway et al., 2016b), past warm intervals (Holloway et al., 2016a; Tindall and Haywood, 2015), as well as present day (Tindall et al., 2009). The representation of the distribution of isotopes in the atmosphere and ocean shown by the model is reasonable (Tindall et al., 2009, 2010) (see Appendix A for a more detailed description of how HadCM3 performs across Greenland).

2.2. Experimental setup – isotopic simulations

HadCM3 is used to simulate the isotopic response to different sea ice retreat scenarios. We perform snapshot simulations, representative of 125 ka conditions. All LIG climate model simulations are driven with greenhouse gas concentrations and orbital parameters for 125 ka and compared to a pre-industrial (PI) control experiment, driven with greenhouse gas values and orbital parameters for 1850-years before present (BP). All experiments are run with a pre-industrial ice-sheet distribution (US Navy 10' dataset - see unified model documentation No 70 by Jones, 1995). Each of the 70-year long LIG sea ice sensitivity experiments are continued from a 200-year long spin-up of a 125 ka control simulation. The 200-year long spin up ensures quasi-equilibrium conditions between the atmosphere and the upper ocean.

To test whether NH sea ice retreat was responsible for the Greenland LIG isotope peak, we perform a suite of experiments each with a different reduction in Arctic sea ice extent. To generate the sea ice retreats, we apply the same method previously used by Holloway et al. (2016a) and implement heat fluxes (from 0 W m^{-2} up to 300 W m^{-2}) to the bottom of the NH sea ice. No other effects are applied to the model physics. That is, the sea ice specific heat flux forcing is kept constant during the whole annual cycle, so the seasonal cycle of sea ice decay and growth is still calculated by the model. The atmosphere and ocean components respond to sea ice variations and sea ice thus changes over time with the coupled model. A full list of experiments is shown in supplementary table 2. A total of 22 experiments have been conducted with different sea ice scenarios each forced by a sea ice heat flux from between 0 to 300 W m-

^{2}. This approach explores the impact of forced arctic sea ice changes on the $\delta^{18}O$ signal across Greenland.

2.3. Model-Data Comparison

2.3.1. Greenland ice core data

To evaluate the impact of different sea ice configurations on the $\delta^{18}O$ ice core record, the model results are compared to the $\delta^{18}O$ values in LIG ice layers. These layers have been identified near the bedrock of seven Greenland deep ice cores: NEEM (NEEM community members, 2013), NGRIP (NGRIP members, 2004), GISP2 (Grootes et al., 1993), GRIP (GRIP members, 1993), Camp Century (Dansgaard et al., 1969), Renland (Johnsen et al., 2001) and DYE-3 (Dansgaard et al., 1982) (Johnsen and Vinther, 2007; NEEM community members, 2013; figure 1 and table 3).

The bottom of the DYE-3, Camp Century, Renland, GRIP and GISP2 ice cores is affected by stratigraphic disturbances and cannot be unambiguously datable (e.g. Johnsen et al. 2001; Grootes et al. 1993; Landais et al. 2003). While the NGRIP core does not cover the entire LIG, its stratigraphy is believed to be well preserved all the way to bedrock due to melting at bed (NGRIP members 2004). Peak NGRIP LIG $\delta^{18}O_{ice}$ values were 3.1‰ higher than present day (Johnsen and Vinther 2007).

The recent deep drilling at NEEM yielded an 80 m section of ice in stratigraphic order, in between disturbed layers. It extends the Greenland $\delta^{18}O$ record back to ~128.5 ka (NEEM community members, 2013). At 126 ka, $\delta^{18}O_{ice}$ values were estimated to be 3.6‰ higher than preindustrial local values at the NEEM deposition site (around 205±20 km upstream of the NEEM drilling site; NEEM community members, 2013). The NEEM community members (2013) used the Holocene isotope-temperature relationship of 0.5 ‰/°C (calibrated using borehole temperature data from other Greenland ice cores; Vinther et al., 2009) to translate the

3.6‰ anomaly into a local warming of 7.5 ± 1.8 °C. After accounting for ice sheet elevation changes and upstream effects, this resulted in a reconstruction of a 8±4°C warming compared to the last millennium (NEEM community members, 2013). Using an alternative method based on measurements of the ice core air isotopic composition ($\delta^{15}N$), Landais et al. (2016) deduce a similar surface temperature warming at NEEM of 8±2.5°C at 126 ka. Note that this latter estimate does not account for ice sheet altitude changes.

2.3.2. <u>Sea surface temperature observations</u>

Syntheses of maximum LIG surface temperature based on ice, marine and terrestrial archives (Turney and Jones, 2010; McKay et al. 2011) have been until recently used for model evaluation (e.g. Lunt et al. 2013, Sime et al. 2013). However given that the warming was not synchronous globally (e.g. Govin et al. 2012, Bauch and Erlenkeuser, 2008), these syntheses do not provide a realistic representation of the LIG climate nor a specific time slice.

More recent compilations by Capron et al. (2014) and Hoffman et al. (2017) have developed harmonized chronologies for paleoclimatic records to produce a spatio-temporal representation of the LIG climate. Capron et al. (2014; 2017) produced five 2000 year long time slices of high-latitude (above 60°N and 60°S) air and sea surface temperature anomalies centred on 115, 120, 125, 127 and 130 ka. Hoffman et al. (2017) provide time slices of global extent of SST anomalies at 120, 125 and 129 ka. While Capron et al. (2014) gather mainly summer high-latitude SST records, Hoffman et al. (2017) provide annual and summer SST records extending down to the tropics. These two datasets use different reference chronologies and distinct methodologies to deduce temporal surface temperature changes and therefore, should be used as independent data benchmarks (Capron et al., 2017).

Here, we compare our model results with the LIG SST datasets compiled for the time interval 125 ka by Capron et al. (2014) and Hoffman et al. (2017) in the high latitude regions. In order to determine the degree of agreement between model results and data, we calculate the root mean square error (RMSE). We do not consider this analysis as an ideal skill score owing to uneven data coverage. Nevertheless, it provides a first-order estimate of the ability of the model to replicate the observations.

3. Isotopic simulation results

We present results from 22 sea ice scenarios here; In each case climatological averages are determined considering the last 50 years of the simulations and a two-sided Student's t test is used to assess the statistical significant of changes (e.g. von Storch and Zwiers, 2001). In addition we focus on three example scenarios which depict low, medium and high sea ice loss. The example experiments show a winter sea ice reduction (hereafter WSIR) compared to the PI simulation of 7% (WSIR-7), 35% (WSIR-35), and 94% (WSIR-94) (experiments marked in red in supplementary table 2).

3.1. Model performance

We start the results section by reviewing the model sea ice output over the Arctic Ocean. Figure 2 shows the comparison of the PI simulation to gridded observational sea ice data (Meier et al., 2017 and Peng et al., 2013). HadCM3 simulates too little summer sea ice under PI conditions (figure 2f). Over the Labrador, Norwegian, Barents and Bering seas, the comparison reveals too much winter sea ice under PI conditions (figure 2c). The model-data mismatch may partly be attributed to the model sea ice physics. Although HadCM3 produces a fairly realistic simulation of sea ice (as previously described by Gordon et al., 2000), the ice pack is represented by a single ice-thickness category and sea ice dynamics are modelled in a rather simple manner (e.g., sea ice is advected via the ocean surface currents) compared to more recent sea ice models (e.g. CICE sea-ice model). Furthermore, the difference between the modern reference (1979 – 1989 AD) used for the data and the PI reference used for the model may also contribute to the discrepancies between model output and data. For example, during the pre-industrial era, the lower GHG emissions relative to the period 1979-1989 (IPCC, 2013), may have allowed more extensive winter sea ice cover.

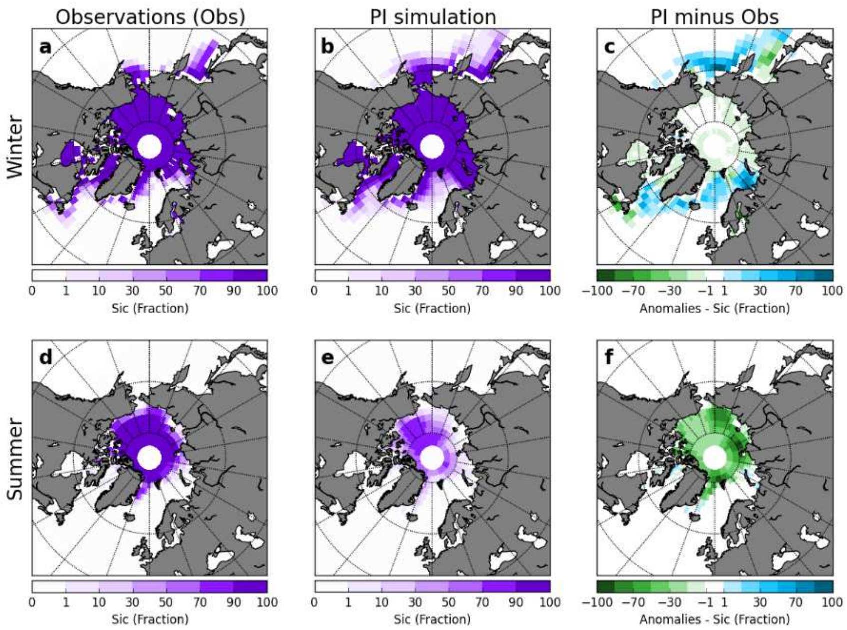

Figure 2. Comparison of the PI simulation to gridded observational sea ice data. Observational data for: (a) winter (March) and (d) summer (September) sea ice concentration (Meier et al., 2017 and Peng et al., 2013). In particular, we use the Goddard Merged sea ice record from 1979 to 1989 (see Meier et al., 2017 and Peng et al., 2013 for more information about the sea ice data). Simulated sea ice concentration for: (b) winter (March) and (e) summer (September) under PI conditions. (c) and (f) show anomalies (PI minus observations) for winter and summer respectively.

3.2. Sea ice extent

For this analysis, we use the standard definition of sea ice extent: the ocean area where sea ice concentration (sic) is at least 15%. Plots of the September and March Arctic sea ice concentrations are presented in figure 3.

For the PI simulation, the mean annual sea ice extent is 12.77 x 10^6 km^2, with a March mean of 18.90 x 10^6 km^2 and a September mean of 5.43 x 10^6 km^2 (table 1). The 125ka control simulation (no sea ice forcing) show a lower September mean (4.05 x 10^6 km^2 - table 1) compared to the PI experiment. This is expected because, during the LIG, larger seasonal and latitudinal insolation variations at the top of the atmosphere (linked to the orbital forcing) resulted in melting of the Arctic sea ice during summer/spring (e.g. Otto-Bliesner et al., 2006).

The 125 ka control simulation with no additional sea ice forcing shows a mean annual sea ice extent of 12.45 x 10^6 km^2. For the LIG sea ice retreat experiments, the annual mean sea ice extent ranges from 9.19 x 10^6 km^2 to 0.63 x 10^6 km^2 depending on the prescribed sea ice forcing (table 1). The lowest March extent (1.18 x 10^6 km^2) is shown by the experiment with the highest sea ice forcing (WSIR-94) (table 1). To calculate the number of ice-free days per year, we consider "nearly ice-free conditions" when the extent of sea ice is less than 10^6 km^2 (IPCC AR5 definition; IPCC, 2013). While the sea ice sensitivity experiments show approximately 83 (WSIR-7), 205 (WSIR-35), 271 (WSIR-94) ice-free days per year, the PI and 125ka control simulations have none.

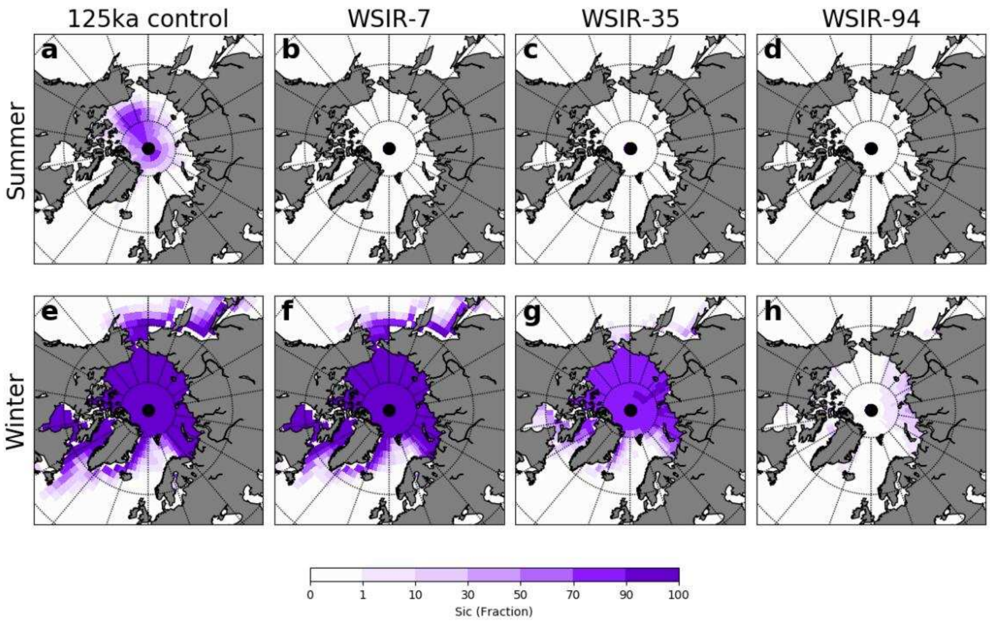

Figure 3. Mean sea ice concentrations (sic - %) for September (first row) and March (second row) for the experiments: 125-ka control (a and e), WSIR-7 (b and f), WSIR-35 (c and g) and WSIR-94 (d and h).

Supplementary figure 1d shows the annual cycle of Arctic sea ice extent in the LIG simulations. The sea ice extent amplitude is 13.47 x 10^6 km^2 and 15.41 x 10^6 km^2 for the PI simulation and 125 ka control simulation respectively (table 1). When simulating the response to a strong sea ice loss (WSIR-94), we obtain a much lower seasonal amplitude of 3.37 x 10^6 km^2 (table 1). WSIR-7 and WSIR-35 experiments show sea ice extent amplitudes of 17.62 x 10^6 km^2 and 12.25 x 10^6 km^2 respectively (table 1).

	PI	**125ka-control**	**WSIR-7**	**WSIR-35**	**WSIR-94**
jan	15.76	16.03	14.60	8.87	2.30
feb	18.00	18.18	16.59	11.94	3.37
mar	18.90	19.46	17.62	12.25	1.18
apr	18.88	19.22	17.35	6.74	0.00
may	16.62	16.87	15.07	0.00	0.00
jun	13.85	13.70	9.93	0.00	0.00
jul	9.54	8.06	1.71	0.00	0.00
aug	6.08	4.59	0.00	0.00	0.00
sep	5.43	4.05	0.00	0.00	0.00
oct	6.53	5.67	0.00	0.00	0.00
nov	10.47	10.25	5.82	0.10	0.06
dec	13.20	13.30	11.58	1.41	0.68
Mean annual extent	**12.77**	**12.45**	**9.19**	**3.44**	**0.63**
Extent amplitude	**13.47**	**15.41**	**17.62**	**12.25**	**3.37**

Table 1. Monthly and annual mean sea ice extent and amplitude of sea ice extent (maximum minus minimum annual sea ice extent) for the PI and selected LIG simulations. Values expressed in 10^6 km^2.

3.3. Sea surface and surface air temperatures

For the 125 ka control simulation with no additional sea ice forcing, there is an increase of NH summer (June-July-August - JJA) temperatures compared to the PI simulation (local increases exceed 3°C – supplementary figure 2c). All sea ice loss experiments reveal an Arctic warming all year round despite reduced winter insolation (supplementary figure 2d to 2l). The Arctic warming, which peaks during the winter months (December-January-February – DJF) (supplementary figure 2e, 2h and 2k), is associated with sea ice retreat, through warmer, expanded ocean waters leading to a warmer atmosphere. This warming impacts the entire circumpolar region, including Greenland.

The large precipitation-weighted air temperature signal reconstructed at the NEEM depositional site of +7.5±1.8°C (8±4°C when accounting for GIS elevation changes) is not reproduced by any of our LIG simulations. At the NEEM deposition site, the experiments

WSIR-7, WSIR-35 and WSIR-94 show precipitation-weighted SAT anomalies of 2.5°C, 3.5°C, 3.0°C respectively, whereas the 125 ka control simulation reveals a more modest warming of 2.1°C relative to the PI control experiment. This underestimation in models of the LIG warming is a discrepancy that has already been extensively discussed in previous studies (e.g. Lunt et al., 2013; Sime et al., 2013).

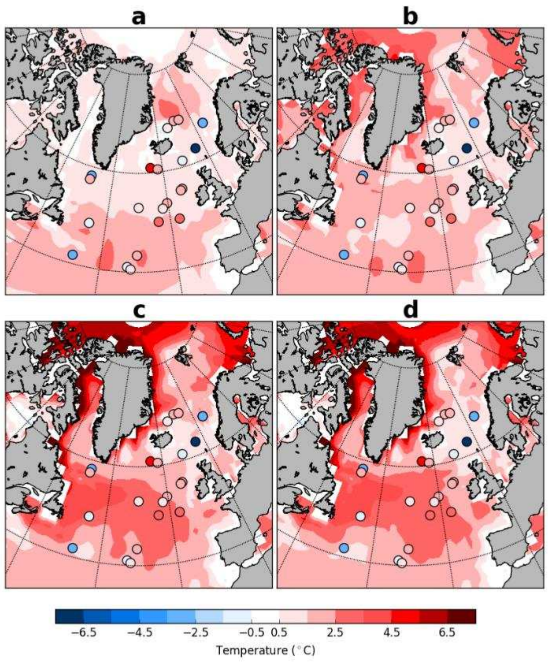

Figure 4. The 125 ka data-based time slice (dots) provided by Capron et al. (2014) superimposed onto modelled summer (JAS) SST anomalies relative to the PI simulation for: (a) 125ka-control (RMSE = 3.0), (b) WSIR-7 (RMSE = 3.0), (c) WSIR-35 (RMSE = 3.2) and (d) WSIR-94 (RMSE = 3.2).

Figure 4 shows results from the 125 ka simulations compared with the 125 ka time slice of Capron et al. (2014). Simulated summer SST anomalies are defined as July-August-September (JAS) to be in agreement with the data of Capron et al. (2014). Considering the uncertainties on SST estimates (±2.6°C on average, see Capron et al., 2014, 2017 for 2σ uncertainty estimates of individual records), the match between the model simulation with no additional sea ice forcing and data is reasonable (figure 4a). When the response to a forced retreat of sea ice is simulated, the agreement with data is very similar than if no sea ice forcing is applied (figure 4b, 4c and 4d). We obtain similar values of RMSE for NH SSTs for all simulations regardless of the sea ice forcing (figure 4). The experiments WSIR-94 and WSIR-35 show the highest RMSE (3.2°C), whereas the 125ka-control and WSIR-7 simulations have the lowest ("best") RMSE (3.0°C) (figure 4). Nevertheless, all simulations fail to reproduce the reconstructed SST anomalies at the sites characterised by cooler-than-present-day conditions irrespective of the sea ice forcing (figure 4). These are located in the Norwegian Sea and in the region south of Greenland. Previous modelling studies (e.g. Capron et al., 2014; Pedersen et al., 2016a) have also difficulties to capture this cooling trend over these regions. Bauch et al. (2012) propose a reduced Atlantic Ocean heat transfer to the LIG Arctic which could explain the regional cooling over the Nordic Seas. And, Langebroek and Nisancioglu (2014) simulate (with the Norwegian Earth System Model - NorESM) cooling conditions over central North Atlantic and Nordic Seas for the LIG, suggesting the simulated climate over these areas may be model dependent.

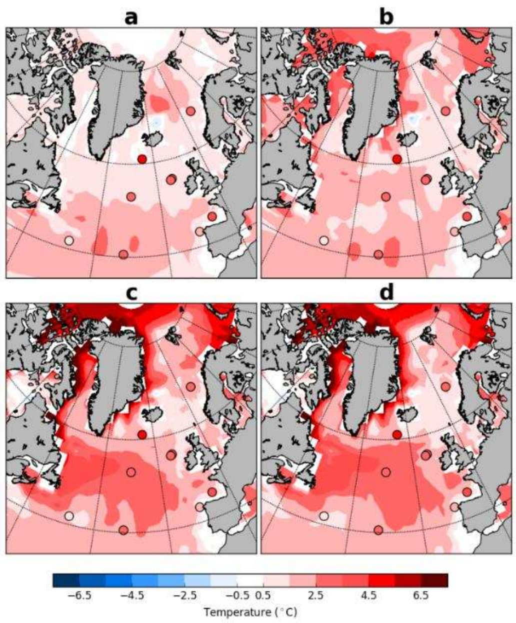

Figure 5. The 125 ka data-based time slice (dots) provided by Hoffman et al. (2017) superimposed onto modelled summer (JAS) SST anomalies relative to PI simulation for: (a) 125ka-control (RMSE = 2.3), (b) WSIR-7 (RMSE = 1.9), (c) WSIR-35 (RMSE = 1.5) and (d) WSIR-94 (RMSE = 1.4). Due to its coastal proximity we exclude MD95-2040 site from our model-data analysis. See Hoffman et al, 2017 for additional information.

In addition, the model results are compared with the 125 time slice from the Hoffman et al. (2017) synthesis. All LIG simulations are generally in good agreement with both summer and annual SST data, considering the uncertainty range related to SST estimates (see Hoffman et al., 2017 for 2σ uncertainty estimates of individual records) (figure 5 and 6). While the experiments with medium and strong sea ice forcing (WSIR-35 and WSIR-94) show the lowest RMSE values ("best" model-data agreement) for both summer (RMSE = 1.5°C and 1.4°C respectively) and annual (RMSE = 1.5°C and 1.4°C respectively) SSTs, the 125ka control simulation reveals the highest RMSE values (2.3°C and 1.9°C for summer and annual SSTs respectively) (figure 5 and 6).

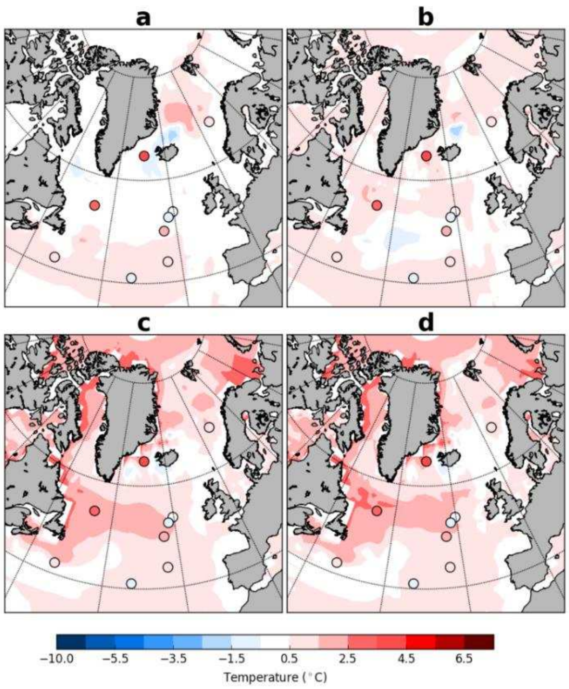

Figure 6. The 125 ka data-based time slice (dots) provided by Hoffman et al. (2017) superimposed onto modelled annual SST anomalies relative to PI simulation for: (a) 125ka-control (RMSE = 1.9), (b) WSIR-7 (RMSE = 1.5), (c) WSIR-35 (RMSE = 1.5) and (d) WSIR-94 (RMSE = 1.4). Due to its coastal proximity we exclude MD95-2040 site from our model-data analysis. See Hoffman et al, 2017 for additional information.

3.4. Response of the hydrological cycle to the sea ice retreat

Annual, winter (DJF) and summer (JJA) averages of Arctic evaporation are shown in figure 7. Directly over areas of reduced Arctic sea ice cover, simulations show an increase in evaporation. Over the Arctic Ocean, all sea ice reduction experiments show an increase in evaporation during both summer and winter compared to the PI simulation (figure 7). When sea ice melts, the replacement of ice at temperatures below zero by open waters, results in a significant increase in evaporation, particularly during the winter months (figure 7h and 7k).

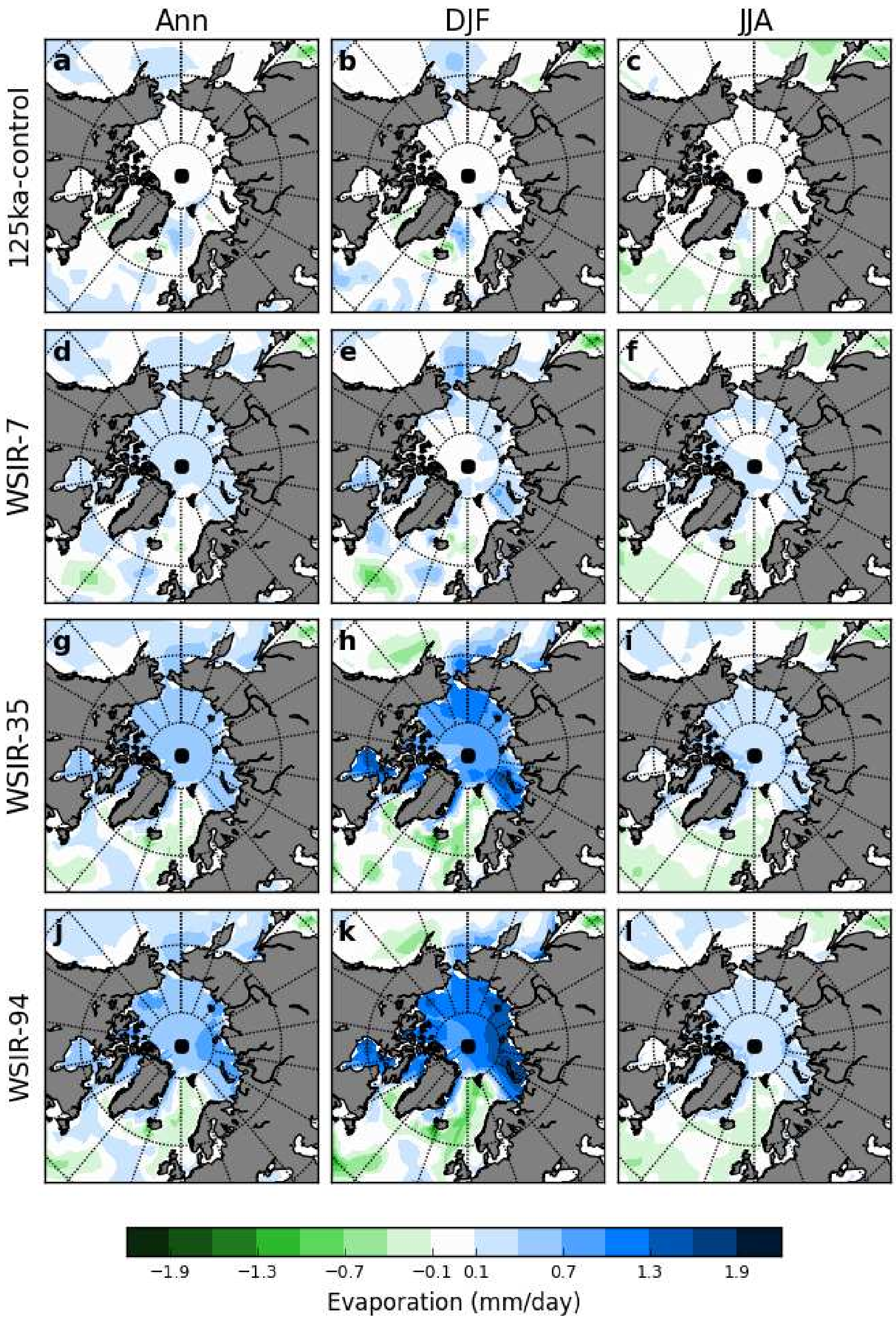

Figure 7. Modelled annual (ann), summer (JJA) and winter (DJF) evaporation anomalies for the 125ka-control simulation (a to c), WSIR-7 (d to f), WSIR-35 (g to i) and WSIR-94 (j to l) compared to the PI simulation. Only the anomalies statistically significant at the 95% confidence level are displayed.

Over the Arctic Basin, local increases in winter evaporation rate exceed 1 mm/day in WSIR-35 and 1.3 mm/day in WSIR-94, while in the low sea ice retreat scenario, WSIR-7, local increases are closer to 0.4 mm/day (figure 7e, 7h, 7k).

The increase in evaporation rate during both summer and winter leads to an increase in precipitation (supplementary figure 3). The ice retreat experiments display similar spatial anomalies, particularly the rise in precipitation in the Arctic Ocean (supplementary figure 3). The increases are more widespread and larger in WSIR-35 and WSIR-94 than in WSIR-7, which is expected considering the larger sea ice loss (supplementary figure 3d-l). The increase in precipitation is greater during the winter months than during summer when precipitation is highest in the Arctic (supplementary figure 3).

A direct atmospheric reaction to sea ice loss and warmer SATs is a decrease in mean sea level pressure (MSLP). The less stable and warmer atmosphere leads to a widespread reduction in winter MSLP over the Arctic Ocean, North Pacific and Bering Sea (supplementary figure 4b-d). Over the Arctic Ocean, local decreases in winter MSLP exceed 200 Pa, 650 Pa and 800 Pa in WSIR-7, WSIR-35 and WSIR-94 respectively (supplementary figure 4b-d).

3.5. Decomposition of $\delta^{18}O$ changes

Ice core records reflect the deposition of snow on the surface, and therefore tend to record climatic information during snow deposition events (e.g. Steig et al., 1994). Hence, precipitation seasonality can cause a recording bias towards those seasons with more snowfall events. Indeed, stable water isotopes in Greenland ice core records have been traditionally compared with precipitation isotopic composition reproduced by isotope-enabled models (e.g. Sime et al., 2013).

In this section, we study how changes in both the monthly isotopic composition of precipitation and the amount of monthly precipitation contribute to the simulated positive $\delta^{18}O$ anomalies at the different Greenland ice core sites (Holloway et al., 2016a; Liu and Battisti, 2015).

To isolate the importance of variations in the seasonal cycle of precipitation (ΔP_{seas}) to the changes in $\delta^{18}O$, we use the following decomposition:

(1) $$\Delta P_{seas} = \frac{\sum_j \delta^{18}O_j^{CONT} * P_j}{\sum_j P_j} - \frac{\sum_j \delta^{18}O_j^{CONT} * P_j^{CONT}}{\sum_j P_j^{CONT}}$$

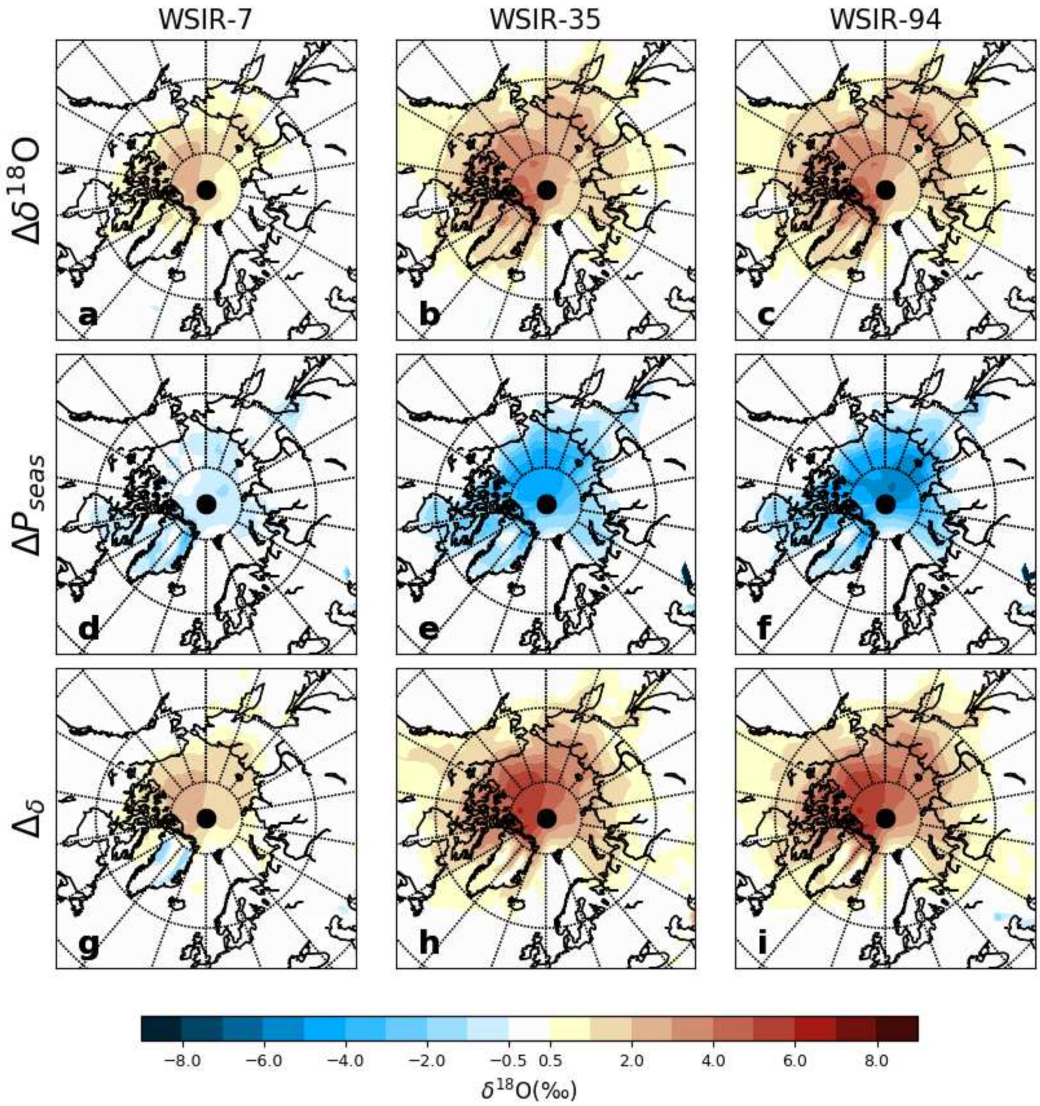

Figure 8. Decomposition of $\delta^{18}O$ changes from 125 ka sea ice retreat experiments. (a,d,g) WSIR-7; (b,e,h) WSIR-35; (c,f,i) WSIR-94. (a-c) The total change in $\delta^{18}O$ ($\Delta\delta^{18}O$). (d-f) The change due to variations in the seasonality of precipitation (ΔP_{seas}). (g-i) The change caused by variations in the $\delta^{18}O$ of precipitation (Δ_δ). Anomalies are calculated compared to the 125 ka control simulation with no additional sea ice forcing.

Superscript CONT denote values from the 125 ka control simulation with no additional sea ice forcing and no superscript denote values from the sea ice sensitivity experiments. The relative impact of other factors (variations in the isotopic composition of precipitate and in the vapor source) contributing to the changes in δ^{18}O is quantified by:

$$(2) \qquad \Delta_{\delta} = \frac{\sum_j \delta^{18}O_j * P_j^{CONT}}{\sum_j P_j^{CONT}} - \frac{\sum_j \delta^{18}O_j^{CONT} * P_j^{CONT}}{\sum_j P_j^{CONT}}$$

Using the monthly δ^{18}O from the 125 ka control simulation and the monthly precipitation of the different sea ice forcing experiments (WSIR-7, WSIR-35 and WSIR-94) (Equation 1), we determine the differences in δ^{18}O due to variations in the seasonal cycle of precipitation (figure 8 d-f). In the same way, using the monthly δ^{18}O from the sea ice retreat experiments (WSIR-7, WSIR-35 and WSIR-94) and the monthly precipitation of the 125 ka control simulation (Equation 2), we isolate the effect of the variations in the isotopic composition of precipitation to the total δ^{18}O changes (figure 8 g-i).

For all sea ice sensitivity experiments (WSIR-7, WSIR-35 and WSIR-94), over the Arctic Ocean and Greenland, ΔP_{seas} is negative (figure 8 d-f) and Δ_{δ} is generally strongly positive (figure 8 g-i). Thus whilst more precipitation falls in the colder months under the sea ice loss scenarios, the increases in δ^{18}O related to the sea ice loss generally outweigh this impact over Greenland.

3.6. Mean annual δ^{18}O changes at the NEEM deposition site

At the NEEM deposition site, the 125-ka control simulation shows a precipitation-weighted δ^{18}O (hereafter $\delta^{18}O_p$) anomaly of 1.7‰ compared to the PI control simulation (figure 9a). This is too low compared to the 3.6‰ increase measured in the NEEM ice core. When the response to a forced retreat of sea ice is simulated, $\delta^{18}O_p$ anomalies rise to between 2.4‰ and 3.9‰ depending on the sea ice forcing prescribed (figure 9b-d and table 2). Simulations with greater than a 17% reduction in winter sea ice best fit the NEEM ice core data (considering the ±1σ uncertainty on the best fit curve - figure 10a).

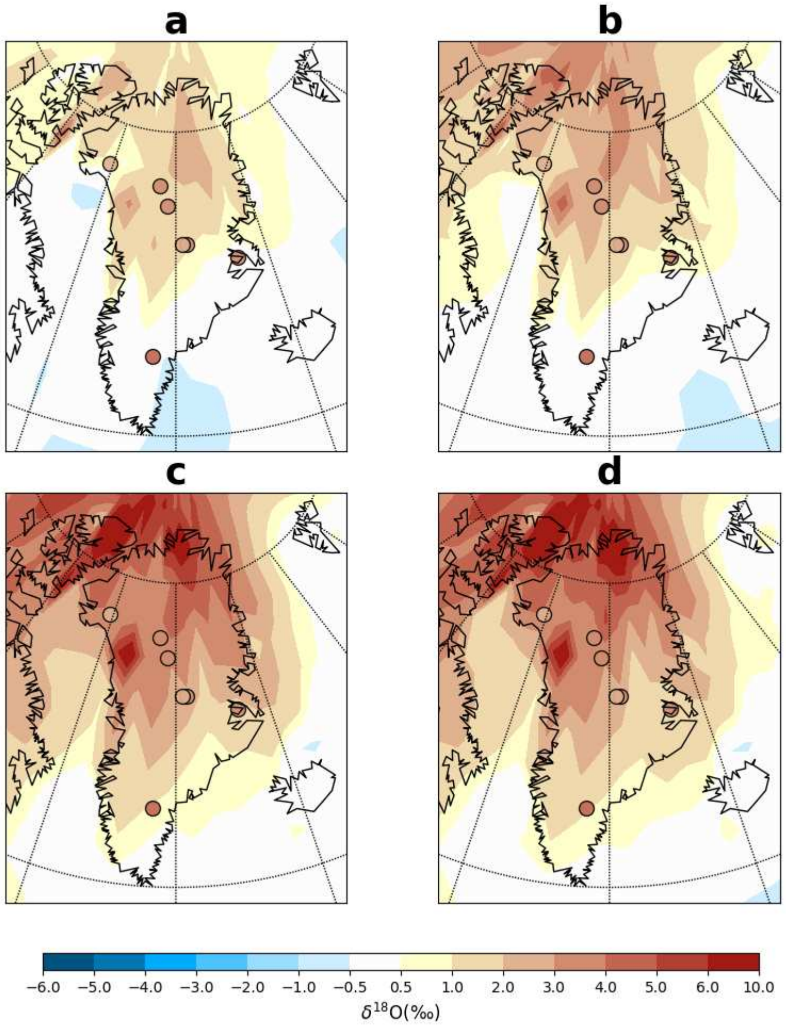

Figure 9. Observed $\delta^{18}O$ anomalies at seven Greenland ice core sites (dots) (Johnsen and Vinther, 2007, NEEM community members, 2013) superimposed onto simulated annual mean precipitation-weighted $\delta^{18}O$ anomalies for: (a) 125ka-control, (b) WSIR-7, (c) WSIR-35 and (d) WSIR-94 compared to the PI simulation.

Exp ID	Precipitation weighted $\delta^{18}O$ (‰)	Precipitation weighted SAT anomalies (°C)	Non-weighted SAT anomalies (°C)
125ka-control	1.7	2.1	0.5
WSIR-7	**2.6**	**2.5**	**0.7**
WSIR-11	2.5	2.9	1.1
WSIR-10	2.4	2.5	1.3
WSIR-15	3.0	3.1	1.6
WSIR-17	3.3	3.5	1.8
WSIR-17b	3.1	3.1	1.7
WSIR-19	2.9	2.6	1.6

WSIR-21	3.2	3.1	1.7
WSIR-22	3.2	3.2	1.7
WSIR-26	3.4	3.0	1.7
WSIR-35	**3.6**	**3.5**	**2.1**
WSIR-41	3.7	3.1	2.2
WSIR-54	3.9	3.5	2.4
WSIR-65	3.5	2.8	2.3
WSIR-72	3.9	3.2	2.2
WSIR-78	3.6	2.9	2.2
WSIR-81	3.6	2.7	1.9
WSIR-89	3.6	2.8	2.1
WSIR-94	**3.7**	**3.0**	**2.3**
WSIR-99	3.5	2.9	2.1
WSIR-100	3.8	3.2	2.1

Table 2. Modelled annual means of precipitation-weighted $\delta^{18}O$, precipitation-weighted SAT and non-weighted SAT anomalies compared to the PI simulation at the NEEM deposition site. Anomalies are listed for each of the 125 ka simulations. The experiments marked in red are the ones mainly discussed in the text.

3.7. Mean annual $\delta^{18}O$ changes at other Greenland ice core sites

The 125-ka control simulation with no additional sea ice forcing shows $\delta^{18}O_p$ anomalies of 1.4‰ at NGRIP and 1.1‰ at GISP2 compared to the PI control simulation (figure 9a and table 3). When forcing a sea ice reduction, simulated $\delta^{18}O_p$ anomalies rise to between 2.0‰ and 3.4‰ at NGRIP and between 1.6‰ and 2.9‰ at GISP2 depending on the sea ice forcing prescribed (figure 9b-d and table 3). At NGRIP and GISP2 sites, LIG $\delta^{18}O$ values were reported to be 3.1‰ and 2.7‰ higher than present day values respectively (Johnsen and Vinther 2007). We find that simulations with a winter sea ice retreat higher than 14% and 16% may explain the NGRIP and GISP2 data respectively (considering the ±1σ uncertainty on the best fit curves - figure 10b and 10g).

At Camp Century site, the sea ice retreat experiments show $\delta^{18}O_p$ anomalies ranging from 1.6‰ to 3.8‰ depending on the sea ice forcing, while the 125ka control simulation reveals a more modest increase in $\delta^{18}O_p$ of 0.5‰ (figure 9 and table 3). Simulations with a winter sea ice reduction between 12% and 28% best fit the $\delta^{18}O$ anomaly of 2.5‰ observed at this location (considering the ±1σ uncertainty on the best fit curve - figure 10e).

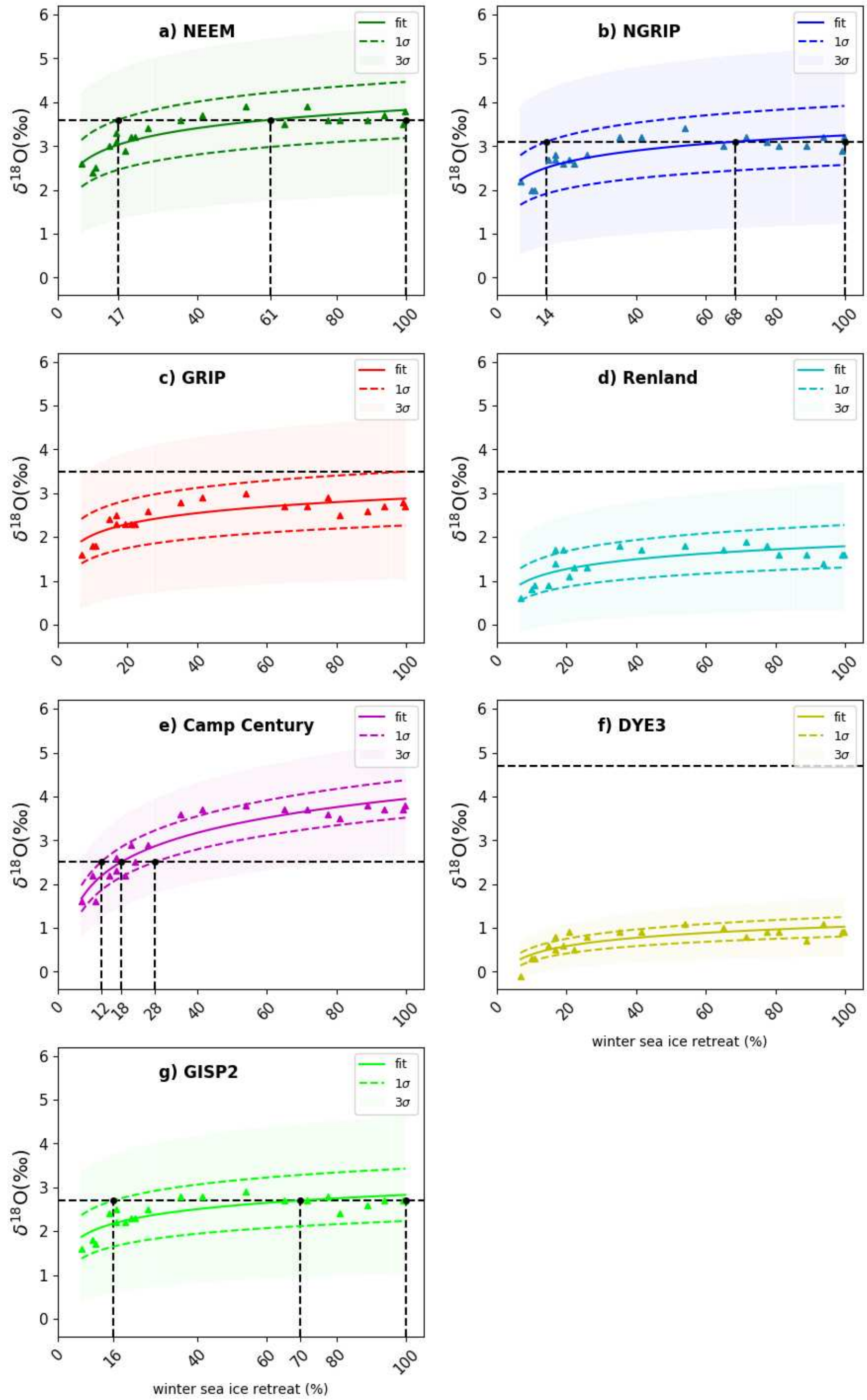

Figure 10. Simulated $\delta^{18}O$ anomalies as a function of winter (March) sea ice retreat. Ice core sites shown: (a) NEEM, (b) NGRIP, (c) GRIP, (d) Renland, (e) Camp Century, (f) DYE3, (g) GISP2. The retreat of sea ice is calculated as the percentage change in winter (March) sea ice extent compared to the PI experiment. Results for each of the 21 sea ice sensitivity experiments are represented by triangles. Solid lines signify best fit lines (fit = b * (log(x) – a)). Also shown $\pm1\sigma$ (lines with dashes) and $\pm3\sigma$ uncertainty (shade envelopes) on the best fit curve. The observed $\delta^{18}O$ anomalies at each ice core site are marked with a black horizontal line with dashes. Black vertical lines with dashes represent the intersections with best fit line and $\pm1\sigma$ uncertainty lines.

	NEEM	NGRIP	GRIP	Renland	Camp Century	DYE3	GISP2
	Observed $\delta^{18}O$ anomalies (‰)						
	3.6	**3.1**	**3.5**	**3.5**	**2.5**	**4.7**	**2.7**
Exp ID	**Modelled $\delta^{18}O$ anomalies (‰)**						
125-ka control	1.7	1.4	1.1	0.2	0.5	-0.3	1.1
WSIR-7	2.6	2.2	1.6	0.6	1.6	-0.1	1.6
WSIR-35	3.6	3.2	2.8	1.8	3.6	0.9	2.8
WSIR-94	3.7	3.2	2.7	1.4	3.7	1.1	2.7

Table 3. Modelled annual mean precipitation-weighted $\delta^{18}O$ anomalies (‰) at seven ice core sites (NEEM, NGRIP, GRIP, Renland Camp Century, DYE3 and GISP2) for selected LIG simulations. Also shown $\delta^{18}O$ anomalies observed in LIG ice relative to present day values reported by NEEM community members, (2013) and Johnsen and Vinther (2007).

At GRIP, Renland and DYE3 sites, LIG $\delta^{18}O$ values were determined to be 3.5‰, 3.5‰, and 4.7‰ higher than present day values respectively (Johnsen and Vinther 2007). Depending on the sea ice forcing, simulated $\delta^{18}O_p$ anomalies vary between 1.6‰ and 3.0‰ at GRIP, between 0.6‰ and 1.9‰ at Renland and between -0.1‰ and 1.1‰ at DYE3 (figure 9 and table 3). Thus, none of our LIG sea ice sensitivity experiments are able to capture the strong $\delta^{18}O$ enrichment reported at these three locations. The underestimated anomalies may be explained by the missing GIS elevation changes in the model runs, or other boundary condition changes not implemented in our simulations, or the uncertainty on both modelled $\delta^{18}O$ values (see appendix B) and ice core measurements. This will be discussed in more detail in section 4.

4. Discussion

4.1. Estimating the Arctic LIG sea ice retreat from Greenland ice core $\delta^{18}O$

Loss of NH sea ice, alongside increased Arctic SSTs, enhances evaporation over the Arctic Ocean and consequently enriches $\delta^{18}O$ values over Greenland. This is a result of isotopically heavy water vapour and a shorter distillation path between the Arctic and Greenland. Thus, in line with previous studies, we have also confirmed that variations in sea ice and sea surface conditions lead to polar impacts on $\delta^{18}O$ (Holloway et al., 2016a; Sime et al., 2013; Sjolte et al., 2014). However, all ice core sites indicate that Greenland $\delta^{18}O$ has a lower sea ice sensitivity as the LIG winter sea ice loss becomes greater than 40-50% (figure 10). This behavior is very likely to be related to the higher sensitivity of Greenland $\delta^{18}O$ to GIS proximal sea ice. Thus when the winter sea ice proximal to Greenland has been lost, $\delta^{18}O$ in Greenland has almost no sensitivity to further sea ice loss. For this reason, whilst Greenland core data allows determination of sea ice change near Greenland, it may not allow insight into the possibility of near complete Arctic LIG sea ice loss.

The seven ice core records, which contain LIG ice, all indicate an increase in $\delta^{18}O$ across Greenland between the present and LIG (Johnsen and Vinther 2007; NEEM community members, 2013). HadCM3 simulations with greater than a 14%, 17% and 16% reduction in winter sea ice extent (compared to the PI simulation) best fit the NGRIP, NEEM and GISP2 LIG $\delta^{18}O$ ice core data. For Camp Century core site, a winter sea ice reduction between 12% and 28% best fits the observed $\delta^{18}O$ anomaly. Our HadCM3 simulations of the response to sea ice retreat undershoot the recorded $\delta^{18}O$ anomalies at Renland, DYE3 and GRIP. Thus we cannot simulate the LIG ice core $\delta^{18}O$ at these sites solely via a forced retreat of Arctic sea ice: the model used here may not be adequately capturing the features at Renland due to its coarse spatial resolution, and relatively tiny size of the coastal Renland icecap. Although, that said, the summertime sea ice pack is too small in the PI simulation; a larger PI summer sea ice pack would increase the potential size of the LIG $\delta^{18}O$ anomaly, likely somewhat improving the model-data match at Renland, DYE3, and GRIP.

The existing observations of LIG Arctic sea ice cover are sparse and not quantitative. Moreover, there is not a current consensus on the presence of perennial (Stein et al., 2017) or seasonal sea ice cover (e.g. Adler et al. 2009; Brigham-Grette and Hopkins, 1995; Spielhagen et al., 2004) over the central LIG Arctic Ocean in the marine core literature. Thus going beyond a qualitative agreement on sea ice retreat between our LIG sea ice results and current marine data is difficult. Additional marine core data, which helps establish the maximum extent of the

LIG sea ice retreat, would be particularly valuable to further evaluate our quantitative sea ice retreat reconstruction.

4.2. What caused this LIG Arctic sea ice retreat?

Proxy data indicate that it is likely that in contrast to present day, there was both reduced winter and summer sea ice extent during the LIG (e.g. Brigham-Grette and Hopkins, 1995; Stein et al., 2017). However, our 125 ka control simulation, forced by GHG and orbital changes, actually shows a 3% increase in winter sea ice and only a rather tiny reduction in the summer sea ice. Many GCMs also have difficulty in accurately capture recent changes in the Arctic sea ice that has occurred during the past decades (e.g. Stroeve et al., 2007, 2012). Thus factors behind the inaccurate representation of historical sea ice variations by GCMs could indicate deficiencies in model physics, for example in the simulation of ocean circulation and heat changes, and/or possible over-simplifications of sea ice model physics e.g. schemes of sea-ice albedo parameterization (e.g. Stroeve et al., 2012). These issues can all affect the simulation of sea ice loss (or increase). However, that said, we believe it is more likely that the LIG retreat of Arctic sea ice was caused by long term changes in meltwater influences over the course of Termination 2 (T2) and the LIG, and subsequent changes of oceanic heat flows into the North Atlantic and Arctic (Capron et al., 2014; Stone et al., 2016).

Capron et al (2014) demonstrate that meltwater from the NH deglaciation likely cooled the Atlantic early in the LIG, enabling better simulation of LIG marine core SST data. A possible subsequent build-up of heat, that was a likely consequence of this early LIG NH meltwater (Capron et al., 2014; Stone et al., 2016), in the rest of the global ocean, and later advection of excess heat to the North Atlantic could then have created the conditions that gave rise of the retreat of 125 ka LIG sea ice. However few, if any, sufficiently long GCM simulations with NH meltwater have been attempted for the LIG. In addition to a lack meltwater forcing, and sufficient duration simulations, there may also be a lack of possible other relevant forcing changes, for example changes in the Bering Strait flow during T2.

4.3. Uncertainties on LIG $\delta^{18}O$ from Greenland ice cores

The sea ice retreat insights provided from our study are dependent on the uncertainties attached to Greenland LIG $\delta^{18}O$ ice core data. Except for the analytical uncertainty (of around 0.1‰), it is indeed not straightforward how to quantify the additional uncertainties that originate from the dating of the LIG layers, the possibility of missing LIG layers and also the lack of constraints on elevation changes at some sites, especially DYE3.

NEEM is the only Greenland ice core where the disturbed bottom ice has been dated with good accuracy. This huge achievement enabled recovery of the first well-dated Greenland LIG record which covered the whole period from 114.5 to 128.5 ka (NEEM community members, 2013). Absolute dating uncertainties on this record are estimated to be around 2000 years (Govin et al., 2015). For the LIG ice at the bottom of other Greenland cores, the dating uncertainties are probably significantly larger. While tentative reconstructions of the chronology of the bottom of the GRIP and GISP2 ice cores have been made using gas record synchronization with Antarctic ice cores (Landais et al, 2003, Suwa et al. 2006), dating the bottom of DYE3 and Camp Century is limited due to the poor preservation of the deep samples. In contrast, the bottom ice stratigraphy at NGRIP is undisturbed so ice dating is much more certain. However for NGRIP, the removal of an older LIG section by basal melt has left a lack of data available to inform glaciological flow modelling used to establish the age model (NGRIP members, 2004), thus again even with this undisturbed ice, the age of the bottom ice is not known any better than 2000 years.

In addition to the dating uncertainties, ice flow can significantly affect ice core $\delta^{18}O$. At some sites the bottom ice has flowed down to the drill site from higher elevation. Thus elevation change between deposition site and drill site adds to the uncertainty of the observed differences between LIG to present day $\delta^{18}O$. Based on total air content analysis it is, believed however that central Greenland elevation was likely unchanged during the LIG (Raynaud et al. 1997), and the Renland LIG ice also very likely originated from elevations very close to present (Johnsen and Vinther 2007).

4.4. <u>Ice sheet, temperature, and wider atmospheric circulation changes</u>

This study focusses on examining the $\delta^{18}O$ signal of Arctic sea ice changes across Greenland, and does not simulate any ice sheet changes, or attempt to reconstruct temperature changes at ice core sites. Nevertheless, we make some comments on GIS, temperature, and wider atmospheric circulation LIG changes.

It has been postulated that the GIS experienced significant change in volume and morphology between the present and LIG (e.g. Church et al., 2013; Dutton et al., 2015). Thus, in addition to sea ice effects, LIG $\delta^{18}O$ signals in Greenland ice cores may also be influenced by changes in the GIS topography. GIS elevation changes would have also affected temperature at ice core sites since lapse rate effects must have occurred, alongside atmospheric circulation and precipitation changes (Merz et al., 2014b). Since most previous studies have suggested that the LIG GIS was smaller than present (e.g. Church et al., 2013; Dutton et al., 2015), this also suggests that larger LIG temperature rises occurred at ice core sites than shown in our simulations, which feature no GIS change.

Previous modelling studies (e.g. Merz et al. 2016; Pederson et al. 2016b; Lunt et al., 2013), all show a smaller warming at NEEM compared to the published values of 8±4°C warming (based on $\delta^{18}O$ data - NEEM community members, 2013) and 8±2.5°C warming (based on $\delta^{15}N$ data - Landais et al., 2016). Our medium sea ice loss (WSIR-35) simulation shows a warming of 3.5°C at the NEEM deposition site. If an additional moderate reduction of NEEM's surface elevation, of 130±300m lower than present (as proposed by the NEEM community members, 2013), were incorporated, an extra warming of around 1.3-4.3°C (assuming an approximate lapse rate of 1°C warmer per 100m height decrease) would occur. This would lead to a possible core site warming of between 4.8°C and 7.8°C.

Note also that the sea ice loss simulations (including WSIR-35) probably underestimate NEEM warming due to 125 ka sea surface condition changes. This is because the simulations exhibit somewhat less Northern Atlantic warming than would be expected due to our method of forcing the model to lose sea ice. Thus further studies examining the joint impacts of GIS change and sea ice change on Greenland, alongside long meltwater influence simulations, would all be most helpful in aiding a better understanding of what drove the LIG Greenland warming.

In terms of atmospheric circulation changes over the wider North Atlantic region, it is also worth noting that sea ice loss and increased temperatures induce a significant drop in MSLP that extends well into the North Pacific. These variations also modify precipitation patterns over the whole Arctic region.

5. Conclusions

In conclusion, this study is a useful complement to previous LIG modelling studies. It highlights the importance of understanding the impact of NH sea ice changes on the LIG Greenland isotopic maximum. Our results show, for the first time, that variations in NH sea ice conditions can lead to substantial LIG Greenland $\delta^{18}O$ increases which are commensurate with $\delta^{18}O$ anomalies observed at NEEM, NGRIP, GISP2 and Camp Century sites. Further modelling studies looking at the combined impact of a smaller GIS and NH sea ice variations, together with additional LIG Arctic sea ice proxies, may help in understanding outstanding model-data mismatches and in evaluating whether Arctic sea ice retreat is indeed a major factor responsible for the high LIG $\delta^{18}O$ measured in Greenland ice cores.

Acknowledgments

We thank Kira Rehfeld for constructive discussion and Peter Hopcroft for his advice on sea ice forcing. We thank the two reviewers for their constructive comments, which helped improved the manuscript through the review process. IMV acknowledges a NERC GW4+ studentship and support provided through the EPSRC-funded Past Earth Network (Grant number EP/M008363/1). LCS acknowledges additional support provided through grants NE/P009271/1, NE/P013279/1, and NE/J004804/1. EC is funded by the European Union's Seventh Framework Programme for research and innovation under the Marie Skłodowska-Curie grant agreement no 600207. BV has received funding from the European Research Council under the European Community's Seventh Framework Programme (FP7/2007-2013) / ERC grant agreement 610055 as part of the ice2ice project.

Data availability

Access to the Met Office Unified Model source code is available under licence from the Met Office at https://www.metoffice.gov.uk/research/collaboration/um-partnership. The climate model data are available on request from http://www.bridge.bris.ac.uk/resources/simulations.

References

Adler, R.E., Polyak, L., Ortiz, J.D., Kaufman, D.S., Channell, J.E.T., Xuan, C., Grottoli, A.G., Selln, E., Crawford, K.A., 2009. Sediment record from the western Arctic Ocean with an improved Late Quaternary age resolution: HOTRAX core HLY0503-8JPC, Mendeleev Ridge. Global and Planetary Change 68, 18-29. https://doi.org/10.1016/j.gloplacha.2009.03.026.

Bauch, H.A., and Erlenkeuser, H., 2008. A "critical" climatic evaluation of last interglacial (MIS 5e) records from the Norwegian Sea. Polar Res. 27, 135-151. https://doi.org/10.1111/j.1751-8369.2008.00059.x.

Bauch, H.A., Kandiano, E.S., Helmke, J.P., 2012. Contrasting ocean changes between the subpolar and polar North Atlantic during the past 135 ka. Geophys. Res. Lett., 39, L11604. https://doi.org/10.1029/2012GL051800.

Brigham-Grette, J., and Hopkins, D.M., 1995. Emergent-marine record and paleoclimate of the last interglaciation along the northwest Alaskan coast. Quat. Res. 43, 159-173. https://doi.org/10.1006/qres.1995.1017.

Brigham-Grette, J., Hopkins, D.M., Ivanov, V.F., Basilyan, A., Benson, S.L., Heiser, P., Pushkar, V., 2001. Last interglacial (Isotope stage 5) glacial and sea level history of coastal Chukotka Peninsula and St. Lawrence Island, western Beringia. Quat. Sci. Rev. 20, 419-436. https://doi.org/10.1016/S0277-3791(00)00107-4.

CAPE Last Interglacial Project members, 2006. Last Interglacial Acrtic warmth confirms polar amplification of climate change. Quat. Sci. Rev. 25, 1383-1400. https://doi.org/10.1016/j.quascirev.2006.01.033.

Capron, E., Govin, A., Stone, E. J., Masson-Delmotte, V., Mulitza, S., Otto-Bliesner, B., Rasmussen, T. L., Sime, L. C., Waelbroeck, C., Wolff, E., 2014. Temporal and spatial structure of multi-millennial temperature changes at high latitudes during the Last Interglacial. Quat. Sci. Rev. 103, 116-133. https://doi.org/10.1016/j.quascirev.2014.08.018.

Capron, E., Govin, A., Feng, R., Otto-Bliesner, B.L., Wolff, E.W., 2017. Critical evaluation of climate syntheses to benchmark CMIP6/PMIP4 127 ka Last Interglacial simulations in the high-latitude regions. Quat. Sci. Rev. 168, 137-150. https://doi.org/10.1016/j.quascirev.2017.04.019.

Church, J.A., Clark, P.U., Cazenave, A., Gregory, J.M., Jevrejeva, S., Levermann, A., Merrifield, M.A., Milne, G.A., Nerem, R.S., and Nunn, P.D., Payne, A.J., Pfeffer, W.T., Stammer, D., Unnikrishnan, A.S., 2013. Sea level change in Climate Change 2013: The Physical Science Basis, Contribution of Working Group I to the Fifth Assessment Report of the Intergovernmental Panel on Climate Change. [Stocker, T.F., D. Qin, G.-K. Plattner, M. Tignor, S.K. Allen, J. Boschung, A. Nauels, Y. Xia, V. Bex and P.M. Midgley (eds.)]. Cambridge University Press, Cambridge, United Kingdom and New York, NY, USA, 1137-1216.

Cronin, T.M., Gemery, L., Briggs Jr., W.M., Jakobsson, M., Polyak, L., Brouwers, E.M., 2010. Quaternary Sea-ice history in the Arctic Ocean based on a new Ostracode sea-ice proxy. Quat. Sci. Rev. 29, 3415-3429. https://doi.org/10.1016/j.quascirev.2010.05.024.

Dansgaard, W., 1964. Stable isotopes in precipitation. Tellus 16, 436-468.

Dansgaard, W., Johnsen S.J., Moller, J., Langway, C.C., 1969. One thousand centuries of climatic record from Camp Century on the Greenland ice sheet. Science, 166, 377-381. https://doi.org/10.1126/science.166.3903.377.

Dansgaard, W., Clausen, H. B., Gundestrup, N., Hammer, C. U., Johnsen, S. J., Kristinsdottir, M., Reeh, N., 1982. A New Greenland Deep Ice Core. Science, 218, 1273-1277. https://doi.org/10.1126/science.218.4579.1273.

Dutton, A., Carlson, A. E., Long, A. J., Milne, G. A., Clark, P. U., DeConto, R., Horton, B. P., Rahmstorf, S., Raymo, M. E., 2015. Sea-level rise due to polar ice-sheet mass loss during past warm periods. Science, 349, 6244. https://doi.org/10.1126/science.aaa4019.

Gierz, P., Werner, M., Lohmann, G., 2017. Simulating climate and stable water isotopes during the Last Interglacial using a coupled climate-isotope model. J. Adv. Model. Earth Syst., 9, 2027-2045. https://doi.org/10.1002/2017MS001056

Gordon, C., Cooper, C., Senior, C. A., Banks, H., Gregory, J. M., Johns, T. C., Mitchell, J. F. B., Wood, R. A., 2000. The simulation of SST, sea ice extents and ocean heat transports in a version of the Hadley Centre coupled model without flux adjustments. Clim. Dynam, 16, 147-168. https://doi.org/10.1007/s003820050010.

Govin, A., Braconnot, P., Capron, E., Cortijo, E., Duplessy, J.-C., Jansen, E., Labeyrie, L., Landais, A., Marti, O., Michel, E., Mosquet, E., Risebrobakken, B., Swingedouw, D., and Waelbroeck, C., 2012. Persistent influence of ice sheet melting on high northern latitude climate during the early Last Interglacial. Clim. Past 8, 483-507. https://doi.org/10.5194/cp-8-483-2012.

Govin, A., Capron, E., Tzedakis, P.C., Verheyden, S., Ghaleb, B., Hillaire-Marcel, C., St-Onge, G., Stoner, J.S., Bassinot, F., Bazin, L., Blunier, T., Combourieu-Nebout, N., El Ouahabi, A., Genty, D., Gersonde, R., Jimenez-Amat, P., Landais, A., Martrat, B., Masson-Delmotte, V., Parrenin, F., Seidenkrantz, M.-S., Veres, D., Waelbroeck, C., Zahn, R., 2015. Sequence of events from the onset to the demise of the Last Interglacial: Evaluating strengths and limitations of chronologies used in climatic archives. Quat. Sci. Rev. 129, 1-36. https://doi.org/10.1016/j.quascirev.2015.09.018.

GRIP members, 1993. Climate instability during the last interglacial period recorded in the GRIP ice core. Nature, 364, 203-207. https://doi.org/10.1038/364203a0.

Grootes, P. M., Stuiver, M., White, J. W. C., Johnsen, S. J., Jouzel, J., 1993. Comparison of oxygen isotope records from the GISP2 and GRIP Greenland ice cores. Nature, 366, 552–554. https://doi.org/doi:10.1038/366552a0.

Hoffman, J.S., Clark, P.U., Parnell, A.C., He, F., 2017. Regional and global sea-surface temperatures during the last interglaciation. Science 355, 276-279. https://doi.org/10.1126/science.aai8464.

Holloway, M.D., Sime, L.C., Singarayer, J.S., Tindall, J.C., Bunch, P., Valdes, P.J., 2016a. Antarctic last interglacial isotope peak in response to sea ice retreat not ice-sheet collapse. Nature communications, 7, 12293. https://doi.org/10.1038/ncomms12293.

Holloway, M.D., Sime, L.C., Singarayer, J.S., Tindall, J.C., Valdes, P.J., 2016b. Reconstructing paleosalinity from $\delta^{18}O$: Coupled model simulations of the Last Glacial Maximum, Last Interglacial and Late Holocene. Quat. Sci. Rev., 131, 350-364. https://doi.org/10.1016/j.quascirev.2015.07.007.

Holloway, M.D., Sime, L.C., Allen, C.S., Hillenbrand, C., Bunch, P., Wolff, E., Valdes, P.J., 2017. The spatial structure of the 128 ka Antarctic sea ice minimum. Geophys. Res. Lett., 44, 11129–11139. https://doi.org/10.1002/2017GL074594.

Howell, F.W., Haywood, A.M., Dolan, A.M., Dowsett, H.J., Francis, J.E., Hill, D.J., Pickering, S.J., Pope, J.O., Salzmann, U. Wade, B.S., 2014. Can uncertainties in sea ice albedo reconcile patterns of data-model discord for the Pliocene and 20th/21st centuries? Geophys. Res. Lett., 41, 2011-2018. https://doi.org/10.1002/2013GL058872.

IPCC, 2013. Climate Change 2013: The Physical Science Basis. Contribution of Working Group I to the Fifth Assessment Report of the Intergovernmental Panel on Climate Change [Stocker, T.F., D. Qin, G.-K. Plattner, M. Tignor, S.K. Allen, J. Boschung, A. Nauels, Y. Xia, V. Bex and P.M. Midgley (eds.)]. Cambridge University Press, Cambridge, United Kingdom and New York, NY, USA, 1535 pp.

Johnsen, S. J., Dahl-Jensen, D., Gundestrup, N., Steffensen, J. P., Clausen, H. B., Miller, H., Masson-Delmotte, V., Sveinbjörnsdottir, A. E., White, J., 2001. Oxygen isotope and palaeotemperature records from six Greenland ice-core stations: Camp Century, Dye-3, GRIP, GISP2, Renland and NorthGRIP, J. Quat. Sci., 16, 299-307. https://doi.org/10.1002/jqs.622.

Johnsen, S. and Vinther, B. 2007. Ice core records – Greenland stable isotopes, in: Elias, S.A., (Eds), Encyclopedia of Quaternary Science., Elsevier, Oxford, pp. 1250-1258.

Jones, C.P., 1995. Unified model documentation paper No 70. Specification of ancillary fields by C P Jones. Version 4 dated 04/12/95.

Jouzel, J., Koster, R.D., Suozzo, R.J., Russell, G.L., 1994. Stable water isotope behaviour during the last glacial maximum: a general circulation model analysis. J. Geophys. Res. 99, 25791-25801. https://doi.org/10.1029/94JD01819.

Jouzel, J., Alley, R.B., Cuffey, K.M., Dansgaard, W., Grootes, P., Hoffmann, G., Johnsen, S.J., Koster, R.D., Peel, D., Shuman, C., Stievenard, M., Stuiver, M., White, J., 1997. Validity of the temperature reconstruction from water isotopes in ice cores. J. Geophys. Res. 102, 26471-26487. https://doi.org/10.1029/97JC01283.

Kopp, R.E., Simons, F.J., Mitrovica, J.X., Maloof, A.C., Oppenheimer, M., 2009. Probabilistic assessment of sea level during the last interglacial stage. Nature 462, 863-867 http://dx.doi.org/10.1038/nature08686.

Langebroek, P.M., Nisancioglu, K.H., 2014. Simulating last interglacial climate with NorESM: role of insolation and greenhouse gases in the timing of peak warmth. Clim, Past, 10, 1305-1318. http://dx.doi.org/10.5194/cp-10-1305-2014.

Landais, A., Chappellaz, J., Delmotte, M., Jouzel, J., Blunier, T., Bourg, C., Caillon, N., Cherrier, S., Malaizé, B., Masson-Delmotte, V., Raynaud, D., Schwander, J., Steffensen, J.P., 2003. A tentative reconstruction of the last interglacial and glacial inception in Greenland based on new gas measurements in the Greenland Ice Core Project (GRIP) ice core. J. Geophys. Res., 108, D18, 4563. https://doi.org/10.1029/2002JD003147.

Landais, A., Masson-Delmotte, V., Capron, E., Langebroek, P. M., Bakker, P., Stone, E. J., Merz, N., Raible, C. C., Fischer, H., Orsi, A., Prié, F., Vinther, B., Dahl-Jensen, D., 2016. How warm was Greenland during the last interglacial period? Clim. Past, 12, 1933-1948. http://dx.doi.org/10.5194/cp-12-1933-2016.

Lunt, D. J., Abe-Ouchi, A., Bakker, P., Berger, A., Braconnot, P., Charbit, S., Fischer, N., Herold, N., Jungclaus, J. H., Khon, V. C., Krebs-Kanzow, U., Langebroek, P. M., Lohmann, G., Nisancioglu, K. H., Otto-Bliesner, B. L., Park,W., Pfeiffer, M., Phipps, S. J., Prange, M., Rachmayani, R., Renssen, H., Rosenbloom, N., Schneider, B., Stone, E. J., Takahashi, K., Wei, W., Yin, Q., Zhang, Z. S., 2013. A multi-model assessment of last interglacial temperatures, Clim. Past, 9, 699-717. http://dx.doi.org/10.5194/cp-9-699-2013.

Liu, X., and Battisti, D. S., 2015. The influence of orbital forcing of tropical insolation on the climate and isotopic composition of precipitation in South America. J. of Climate, 28(12), 4841-4862. https://doi.org/10.1175/JCLI-D-14-00639.1

McKay, N. P., Overpeck, J. T., Otto-Bliesner, B. L., 2011. The role of ocean thermal expansion in Last Interglacial sea level rise. Geophys. Res. Lett., 38, L14605. http://dx.doi.org/10.1029/2011GL048280.

Masson-Delmotte, V., Jouzel, J., Landais, A., Stievenard, M., Johnsen, S.J., White, J.W.C., Werner, M., Sveinbjornsdottir, A., Fuhrer, K., 2005. GRIP deuterium excess reveals rapid and orbital-scale changes in Greenland moisture origin. Science. 309(5731), 118-121. http://dx.doi.org/10.1126/science.1108575.

Masson-Delmotte, V., Braconnot, P., Hoffmann, G., Jouzel, J., Kageyama, M., Landais, A., Lejeune, Q., Risi, C., Sime, L. C., Sjolte, J., Swingedouw, D., Vinther, B. M., 2011. Sensitivity of interglacial Greenland temperature and $\delta^{18}O$: ice core data, orbital and increased CO_2 climate simulations. Clim. Past, 7, 1041-1059. http://dx.doi.org/10.5194/cp-7-1041-2011.

Masson-Delmotte, V., Schulz, M., Abe-Ouchi, A., Beer, J., Ganopolski, A., González Rouco, J. F., Jansen, E., Lambeck, K., Luterbacher, J., Naish, T., Osborn, T., Otto-Bliesner, B., Quinn, T., Ramesh, R., Rojas, M., Shao, X., Timmermann, A., 2013. Information from Paleoclimate Archives, in: Climate Change 2013: The Physical Science Basis. Contribution of Working Group I to the Fifth Assessment Report of the Intergovernmental Panel on Climate Change. [Stocker, T.F., D. Qin, G.-K. Plattner, M. Tignor, S.K. Allen, J. Boschung, A. Nauels, Y. Xia, V. Bex and P.M. Midgley (eds.)]. Cambridge University Press, Cambridge, United Kingdom and New York, NY, USA, 383-464.

Meier, W., F. Fetterer, M. Savoie, S. Mallory, R. Duerr, J. Stroeve. 2017. NOAA/NSIDC Climate Data Record of Passive Microwave Sea Ice Concentration, Version 3. Goddard Merged sea ice record from 1979 to 1989. Boulder, Colorado USA. NSIDC: National Snow and Ice Data Center. http://dx.doi.org/10.7265/N59P2ZTG. 17/10/2017.

Merz, N., Born, A., Raible, C. C., Fischer, H., Stocker, T. F., 2014a. Dependence of Eemian Greenland temperature reconstructions on the ice sheet topography, 2014. Clim. Past, 10, 1221-1238. http://dx.doi.org/10.5194/cp-10-1221-2014.

Merz, N., Gfeller, G., Born, A., Raible, C. C., Stocker, T. F., Fischer, H., 2014b. Influence of ice sheet topography on Greenland precipitation during the Eemian interglacial. J. Geophys. Res., 119, 10749-10768. http://dx.doi.org/10.1002/2014JD021940.

Merz, N., Born, A., Raible, C. C., Stocker, T. F., 2016. Warm Greenland during the last interglacial: the role of regional changes in sea ice cover. Clim. Past, 12, 2011–2031. https://doi.org/10.5194/cp-12-2011-2016.

NEEM community members, 2013. Eemian interglacial reconstructed from a Greenland folded ice core. Nature, 493, 489–494. https://doi.org/10.1038/nature11789.

NGRIP Project Members, 2004. High-resolution record of Northern Hemisphere climate extending into the last interglacial period. Nature 431, 147-151. https://doi.org/10.1038/nature02805.

Nørgaard-Pedersen, N., Mikkelsen, N., Lassen, S.J., Kristoffersen, Y., Sheldon, E., 2007. Reduced sea ice concentrations in the Arctic Ocean during the last interglacial period revealed by sediment cores off northern Greenland. Paleoceanography 22, PA1218. http://dx.doi.org/10.1029/2006PA001283.

Otto-Bliesner, B.L., Marshall, S.J., Overpeck, J.T., Miller, G.H., Hu, A., CAPE Last Interglacial Project members., 2006. Simulating arctic climate warmth and icefield retreat in the Last Interglacial. Science, 311, 1751-1753. http://dx.doi.org/10.1126/science.1120808.

Otto-Bliesner, B., Rosenbloom, N., Stone, E., McKay, N.P., Lunt, D.J., Brady, E.C., Overpeck, J.T., 2013. How warm was the Last Interglacial? New model-data comparisons. Philos. Trans. R. Soc. A Phys. Math. Eng. Sci., 371. http://dx.doi.org/10.1098/rsta.2013.0097.

Pedersen, R.A, Langen, P.L., Vinther, B.M., 2016a. The last interglacial climate: comparing direct and indirect impacts of insolation changes. Clim. Dynam, 48, 3391-3407. http://dx.doi.org/10.1007/s00382-016-3274-5.

Pedersen, R.A, Langen, P.L., Vinther, B.M., 2016b. Greenland during the last interglacial: the relative importance of insolation and oceanic changes. Clim. Past, 12, 1907-1918. http://dx.doi.org/10.5194/cp-12-1907-2016.

Peng, G., Meier, W.N., Scott, D.J., Savoie, M.H., 2013. A long-term and reproducible passive microwave sea ice concentration data record for climate studies and monitoring. Earth Syst. Sci. Data. 5. 311-318. http://dx.doi.org/10.5194/essd-5-311-2013.

Raynaud, D., Chappellaz, J., Ritz, C., Martinerie, P., 1997. Air content along the Greenland Ice Core Project core: A record of surface climatic parameters and elevation in central Greenland. J. Geophys. Res., 102, C12, 26607-26613.

Rehfeld, K., Münch, T., Ho, S.L., Laepple, T., 2018. Global patterns of declining temperature variability from the Last Glacial Maximum to the Holocene. Nature, 554, 356-359. http://dx.doi.org/10.1038/nature25454.

Schmidt, G.A., LeGrande, A.N., Hoffmann, G., 2007. Water isotope expressions of intrinsic and forced variability in a coupled ocean-atmosphere model. J. Geophys. Res., 112, D10103. http://dx.doi.org/10.1029/2006JD007781.

Schmidt, G.A., Annan, J.D., Bartlein, P.J., Cook, B.I., Guilyardi, E., Hargreaves, J.C., Harrison, S.P., Kageyama, M., LeGrande, A.N., Konecky, B., Lovejoy, S., Mann, M.E., Masson-Delmotte, V., Risi, C., Thompson, D., Timmermann, A., Tremblay, L.B., Yiou, P., 2014. Using palaeo-climate comparisons to constrain future projections in CMIP5. Clim. Past, 10, 221-250. http://dx.doi.org/10.5194/cp-10-221-2014.

Sime, L. C., Risi, C., Tindall, J. C., Sjolte, J., Wolff, E. W., Masson-Delmotte, V., Capron, E., 2013. Warm climate isotopic simulations: what do we learn about interglacial signals in Greenland ice cores? Quat. Sci. Rev. 67, 59-80. https://doi.org/10.1016/j.quascirev.2013.01.009.

Sjolte, J., Hofmann, G., Johnsen, S.J., 2014. Modelling the response of stable water isotopes in Greenland precipitation to orbital configurations of the previous interglacial. Tellus B: Chemical and Physical Meteorology, 66, 22872. https://doi.org/10.3402/tellusb.v66.22872

Spielhagen, R. F., Baumann, K., Erlenkeuser, H., Nowaczyk, N. R., Nørgaard-Pedersen, N., Vogt, C., Weiel, D., 2004. Arctic Ocean deep-sea record of Northern Eurasian ice sheet history. Quat. Sci. Rev. 23, 1455-1483. https://doi.org/10.1016/j.quascirev.2003.12.015.

Steffensen, J. P., Andersen, K. K., Bigler, M., Clausen, H. B., Dahl-Jensen, D. and co-authors, 2008. High-resolution Greenland ice core data show abrupt climate change happens in few years. Science. 321(5889), 680-684. https://doi.org/10.1126/science.1157707.

Steig, E. J., Grootes, P. M., Stuiver, M., 1994. Seasonal Precipitation Timing and Ice Core Records. Science, 266, 1885-1886. https://doi.org/10.1126/science.266.5192.1885.

Stein, R., Fahl, K., Gierz, P., Niessen, F., Lohmann., G., 2017. Arctic Ocean sea ice cover during the penultimate glacial and the last interglacial. Nature communications, 8, 373. https://doi.org/10.1038/s41467-017-00552-1.

Stone, E.J., Capron, E., Lunt, D.J., Payne, A.J., Singarayer, J.S., Valdes, P.J., Wolff, E.W., 2016. Impact of meltwater on high-latitude early Last Interglacial climate. Clim. Past, 12, 1919-1932.

Stroeve, J., Holland, M.M., Meier, W., Scambos, T., Serreze, M., 2007. Arctic sea ice decline: Faster than forecast, Geophys. Res. Lett., 34, L09501. https://doi.org/10.1029/2007GL029703.

Stroeve, J.C., Kattsov, V., Barrett, A., Serreze, M., Pavlova, T., Holland, M., Meier, W.N., 2012. Trends in Arctic sea ice extent from CMIP5, CMIP3 and observations, Geophys. Res. Lett., 39, L16502. https://doi.org/10.1029/2012GL052676.

Suwa, M., von Fischer, J.C., Bender, M.L., Landais, A., Brook, E.J., 2006. Chronology reconstruction for the disturbed bottom section of the GISP2 and the GRIP ice cores: Implications for Termination II in Greenland. J, of Geophys. Res., 111, D02101, https://doi.org/10.1029/2005JD006032.

Tindall, J. C., Valdes, P. J. Sime, L. C., 2009. Stable water isotopes in HadCM3: Isotopic signature of El Niño-Southern Oscillation and the tropical amount effect. J. Geophys. Res. 114, D04111. https://doi.org/10.1029/2008JD010825.

Tindall, J. C, Flecker, R., Valdes, P.J., Schimidt, D.N., Markwick, P., Harris, J., 2010. Modelling the oxygen isotope distribution of ancient seawater using a coupled ocean-atmosphere GCM: Implications for reconstructing early Eocene climate. Earth Planet Sci. Lett. 292, 265-273. https://doi.org/10.1016/j.epsl.2009.12.049.

Tindall, J. C., and Haywood, A.L., 2015. Modeling oxygen isotopes in the Pliocene: Large-scale features over the land and ocean. Paleoceanography, 30, 1183-1201. http://dx.doi.org/10.1002/2014PA002774.

Turney, C.S.M., and Jones, R.T., 2010. Does the Agulhas Current amplify global temperatures during super-interglacials? J. Quat. Sci., 25 (6), 839-843. http://dx.doi.org/10.1002/jqs.1423.

Vaughan, D. G., Comiso, J. C., Allison, I., Carrasco, J., Kaser, G., Kwok, R., Mote, P., Murray, T., Paul, F., Ren, J., Rignot, E., Solomina, O., Steffen, K., and Zhang, T., 2013. Observations: Cryosphere, in: Climate Change 2013: The Physical Science Basis, Contribution of Working Group I to the Fifth Assessment Report of the Intergovernmental Panel on Climate Change. [Stocker, T.F., D. Qin, G.-K. Plattner, M. Tignor, S.K. Allen, J. Boschung, A. Nauels, Y. Xia, V. Bex and P.M. Midgley (eds.)]. Cambridge University Press, Cambridge, United Kingdom and New York, NY, USA, 317-382.

Vinther, B. M., Buchardt, S. L., Clausen, H. B., Dahl-Jensen, D., Johnsen, S. J., Fisher, D.A., Koerner, R.M., Raynaud, D., Lipenkov, V., Anderse, K.K., Blunier, T., Rasmussen, S.O., Steffensen, J.P., Svensson, A.M. 2009. Holocene thinning of the Greenland ice sheet. Nature, 461, 385-388. https://doi.org/10.1038/nature08355.

von Storch, H. and Zwiers, F. W., 2001. Statistical Analysis in Climate Research, Cambridge University Press, Cambridge, UK and New York, NY, USA, 111-118 pp.

Werner, M., Langebroek, P.M., Carlsen, T., Herold, M., Lohmann, G., 2011. Stable water isotopes in the ECHAM5 general circulation model: toward high-resolution isotope modeling on a global scale. Journal of Geophysical Research 116, D15109. https://doi.org/doi:10.1029/2011JD015681.

Supplementary information

Table 1. Compilation of observations of NH sea ice changes for the LIG.

Site	Proxy	Comments	Reference
GreenICE (core 11)	Subpolar foraminifers	The presence of subpolar planktonic foraminifers in MIS 5e zone interpreted to indicate reduced sea ice cover compared to present.	Nørgaard-Pedersen et al., 2007
HLY0503-8JPC	Subpolar foraminifers	Subpolar planktonic foraminifers found in MIS 5e zone suggest reduced sea-ice cover, perhaps seasonally ice-free conditions.	Adler et al., 2009
Nome, St. Lawrence Island and Beaufort Sea shelf	Mollusc and ostracode faunas	Fossil assemblages suggest that the winter sea-ice limit did not expand south of Bering Strait, that the Bering Sea was annually ice-free and that the sea ice cover in the Arctic ocean was not perennial for some period.	Brigham-Grette and Hopkins. (1995)
NP26-5/32	Ostracode faunas	Ostracode Acetabulastoma arcticum, which inhabits exclusively in areas of perennial Artic sea ice, occurs during late MIS 5e but it is absent during peak interglacial.	Cronin et al., (2010)
Oden96/12-1pc	Ostracode faunas	Ostracode Acetabulastoma arcticum, which inhabits exclusively in areas of perennial Artic sea ice, occurs during late MIS 5e but it is absent during peak interglacial.	Cronin et al., (2010)
PS2200-5	Ostracode faunas	Ostracode Acetabulastoma arcticum, which inhabits exclusively in areas of perennial Artic sea ice, occurs during late MIS 5e but it is absent during peak interglacial.	Cronin et al., (2010)
	Biomarker proxy IP25, terrestrial biomarkers and open-water phytoplankton biomarkers	Biomarker proxies suggest perennial sea ice cover in the central part of Arctic Ocean during MIS 5e.	Stein et al. (2017)
PS51/038-3	Biomarker proxy IP25, terrestrial biomarkers and open-water phytoplankton biomarkers	Biomarker proxies suggest perennial sea ice cover in the central part of Arctic Ocean during MIS 5e.	Stein et al. (2017)
PS2138-2	Biomarker proxy IP25, terrestrial biomarkers and open-water phytoplankton biomarkers	Biomarker proxies suggest seasonal open-water conditions over the Barents Sea continental margin.	Stein et al. (2017)

PS2757-8	Biomarker proxy IP25, terrestrial biomarkers and open-water phytoplankton biomarkers	Biomarker proxies suggest relatively closed sea ice cover conditions during MIS 5e.	Stein et al. (2017)

Table 2. Full list of simulations. The experiments marked in red are the ones mainly discussed in the text.

Exp ID	Eccentricity	Obliquity (°)	Perihelion (day of yr)	Prescribed heat flux (W m^{-2})	CO_2 (ppmv)	CH_4 (ppbv)	N_2O (ppbv)	Percentage change in March Arctic sea ice extent relative to PI simulation (%)
PI	0.0167	23.45	1.7	0	280	760	270	0
125ka-control	0.04001	23.80	201.3	0	276	640	263	+3
WSIR-7	0.04001	23.80	201.3	15	276	640	263	-7
WSIR-11	0.04001	23.80	201.3	20	276	640	263	-11
WSIR-10	0.04001	23.80	201.3	25	276	640	263	-10
WSIR-15	0.04001	23.80	201.3	30	276	640	263	-15
WSIR-17	0.04001	23.80	201.3	35	276	640	263	-17
WSIR-17b	0.04001	23.80	201.3	40	276	640	263	-17
WSIR-19	0.04001	23.80	201.3	50	276	640	263	-19
WSIR-21	0.04001	23.80	201.3	55	276	640	263	-21
WSIR-22	0.04001	23.80	201.3	60	276	640	263	-22
WSIR-26	0.04001	23.80	201.3	80	276	640	263	-26
WSIR-35	0.04001	23.80	201.3	100	276	640	263	-35
WSIR-41	0.04001	23.80	201.3	120	276	640	263	-41
WSIR-54	0.04001	23.80	201.3	140	276	640	263	-54
WSIR-65	0.04001	23.80	201.3	145	276	640	263	-65
WSIR-72	0.04001	23.80	201.3	150	276	640	263	-72
WSIR-78	0.04001	23.80	201.3	155	276	640	263	-78
WSIR-81	0.04001	23.80	201.3	160	276	640	263	-81
WSIR-89	0.04001	23.80	201.3	180	276	640	263	-89
WSIR-94	0.04001	23.80	201.3	200	276	640	263	-94
WSIR-99	0.04001	23.80	201.3	250	276	640	263	-99
WSIR-100	0.04001	23.80	201.3	300	276	640	263	-100

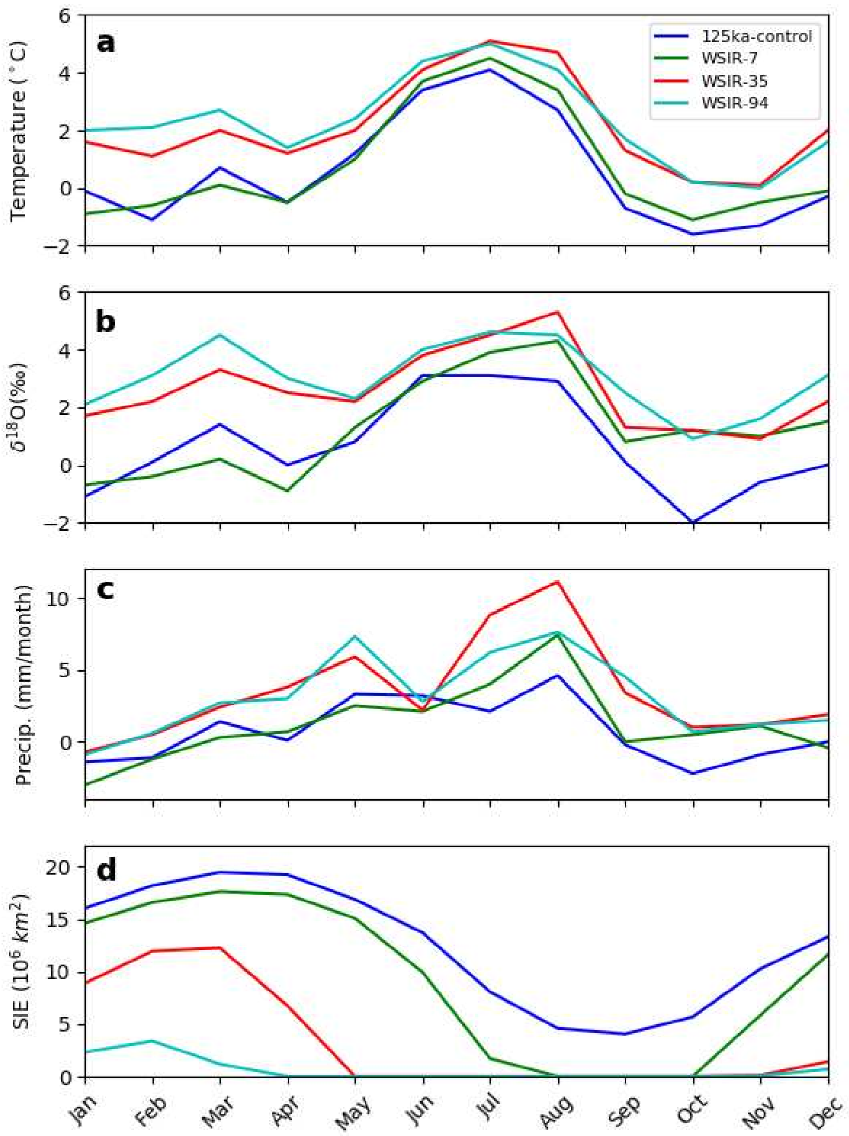

Figure 1. Change in the seasonal cycle of (a) temperature (°C), (b) $\delta^{18}O$ (‰), and (c) precipitation (mm/month) at the NEEM deposition site. Anomalies are calculated between the 125 ka simulations using heat fluxes of 0 W m^{-2} (125ka-control, dark blue), 15 W m^{-2} (WSIR-7, green), 100 W m^{-2} (WSIR-35, red) and 200 W m^{-2} (WSIR-94, cyan) compared to the PI simulation. Also shown the annual cycle of Arctic sea ice extent (SIE – 10^6 km^2) in the LIG simulations.

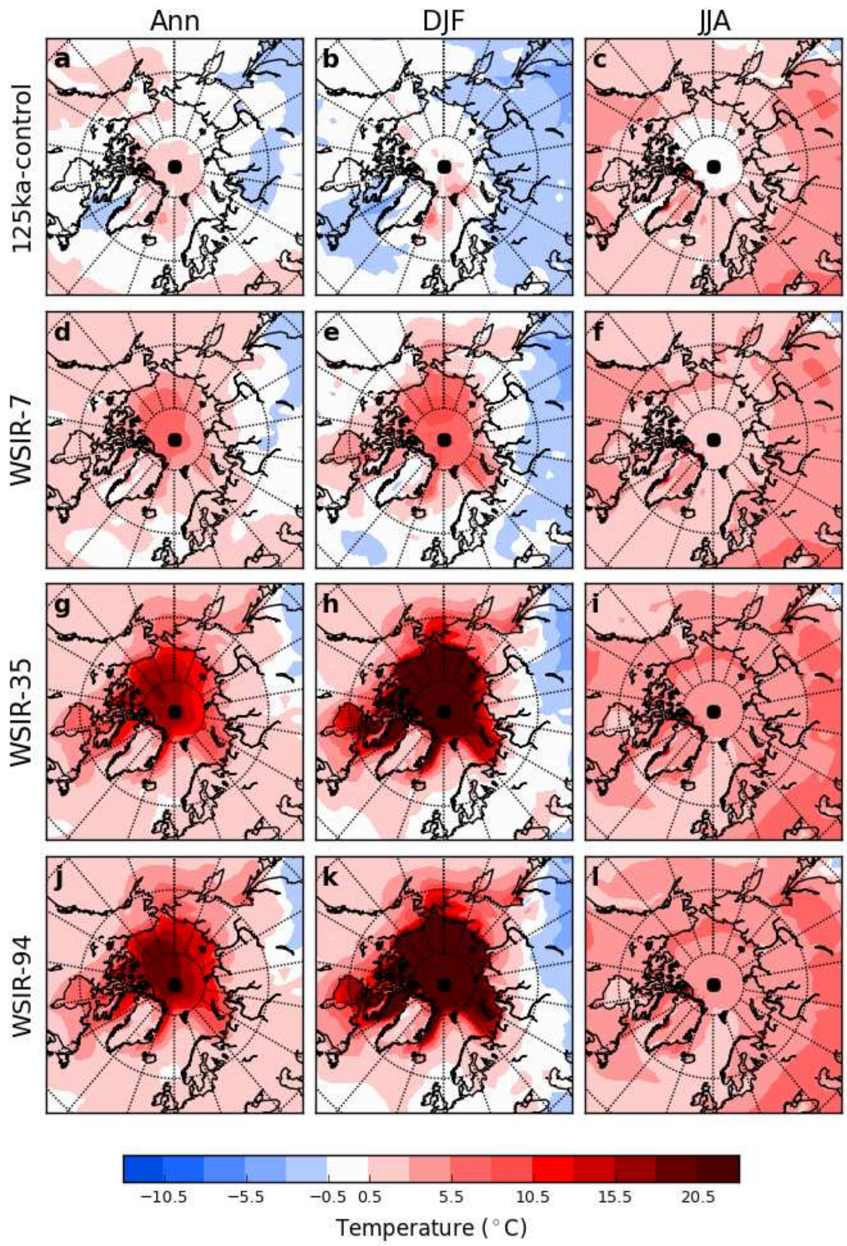

Figure 2. Modelled annual (ann), summer (JJA) and winter (DJF) surface air temperature anomalies for the 125ka-control simulation (a to c), WSIR-7 (d to f), WSIR-35 (g to i) and WSIR-94 (j to l) compared to the PI simulation. Only the anomalies statistically significant at the 95% confidence level are displayed.

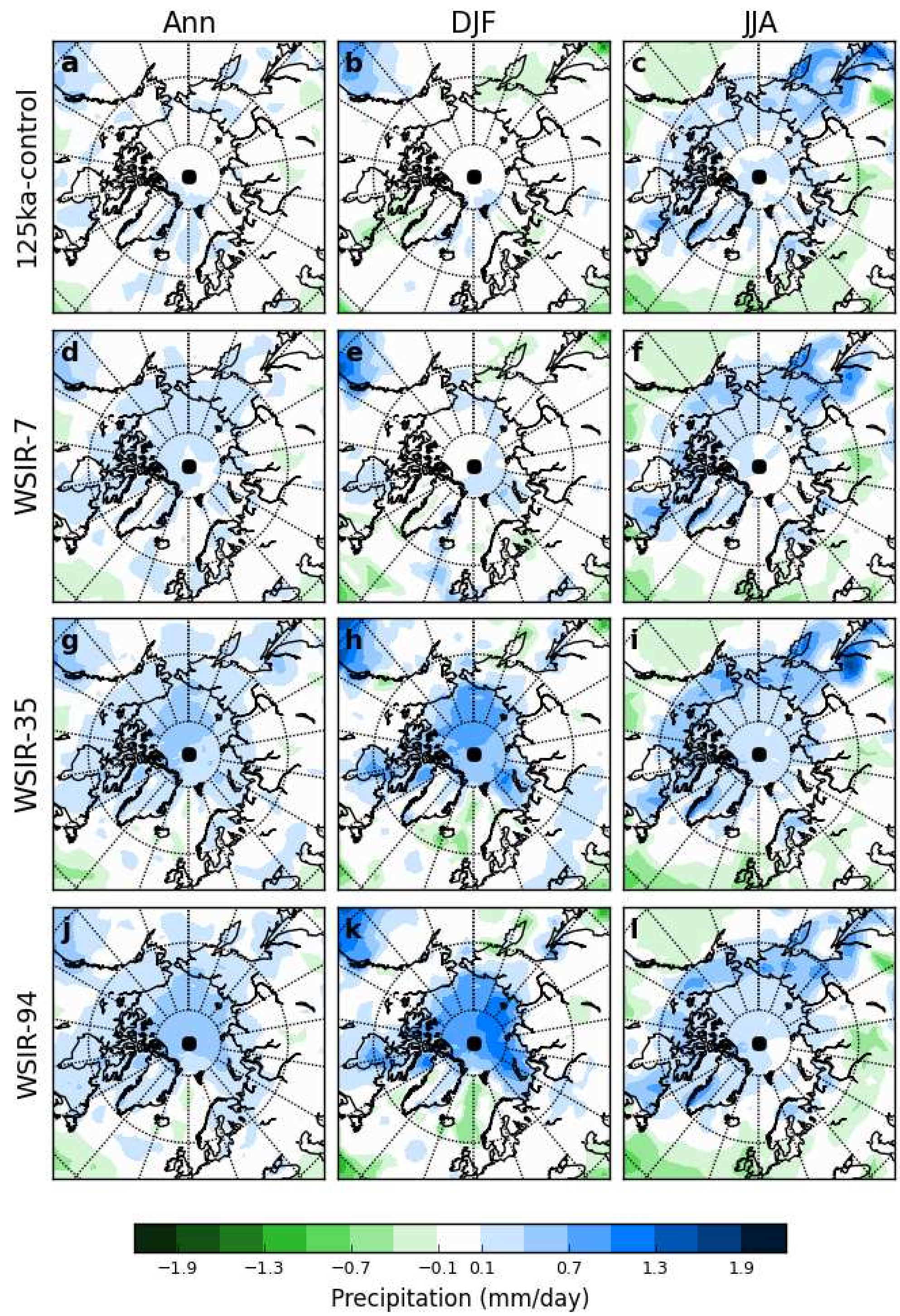

Figure 3. Modelled annual (ann), summer (JJA) and winter (DJF) precipitation anomalies for the 125ka-control simulation (a to c), WSIR-7 (d to f), WSIR-35 (g to i) and WSIR-94 (j to l) compared to the PI simulation. Only the anomalies statistically significant at the 95% confidence level are displayed.

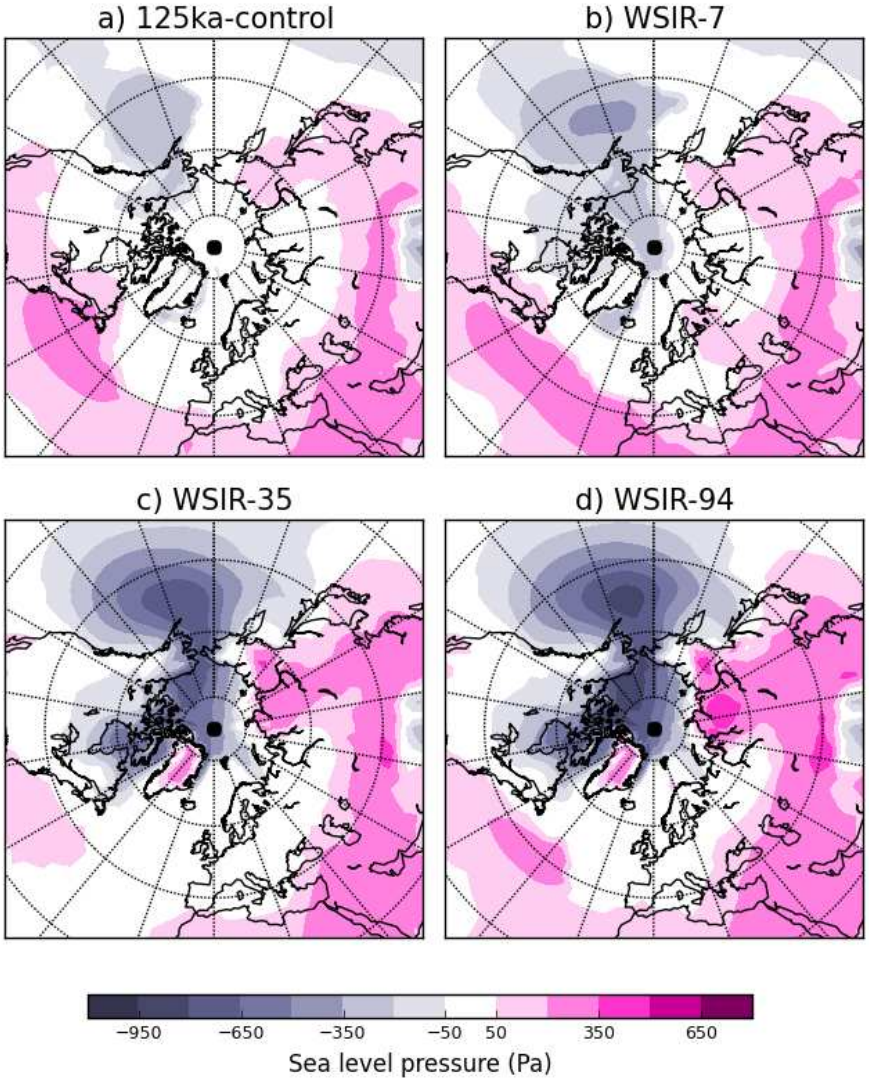

Figure 4. Modelled winter sea level pressure anomalies (Pa) for: a) 125ka-control, b) WSIR-7, c) WSIR-35 and d) WSIR-94 compared to the PI simulation. Only the anomalies statistically significant at the 95% confidence level are displayed.

Appendix A. Model evaluation

In this section, we provide an evaluation of two control (PI and present-day experiments) HadCM3 isotope simulations over Greenland. Previous work by Sime et al. (2013), using the atmosphere only component of this model (HadAM3), has shown that annual Greenland means of both isotopic values and surface temperatures are on average 8.6‰ too heavy and 1.9°C too warm respectively, compared with present-day observations compiled by by Vinther et al. (2010) and Sjolte et al. (2011). Following on from this, HadCM3 surface temperatures and isotopic values are compared with the observational data provided by Vinther et al. (2010) and Sjolte et al. (2011) (see Sime et al., 2013 for estimates and locations of individual records).

Comparison with observations indicates an annual warm bias over Greenland of 2.2°C for the PI simulation and 3.7°C for the present-day simulation (figure A.1b). Note, most observational sites are located in central Greenland, providing an unequal representation of the whole of Greenland. Hence, the comparison can be considered more representative of the cold central Greenland region (see figure A.1b for the position of the observational sites).

The $\delta^{18}O$ results follow a similar pattern (figure A.1a). Comparison with the observations suggests that both the PI and present-day simulations are on average 5.8‰ and 7.1‰ (figure A.1a) too heavy respectively. Some other models show similar heavy $\delta^{18}O$ biases (e.g. Hoffmann et al., 1998; Sjolte et al., 2011; Sime et al., 2013). Sime et al. (2013) point to the inaccurate seasonal representation of the isotopes in precipitation as a possible reason for the model-data isotopic offset.

It would be expected that similar bias affect the PI and LIG simulations. Therefore, to reduce the impact of model bias over Greenland, and hence any effects on the study results, we follow the standard approach of reporting modelled values as anomalies (PI minus LIG).

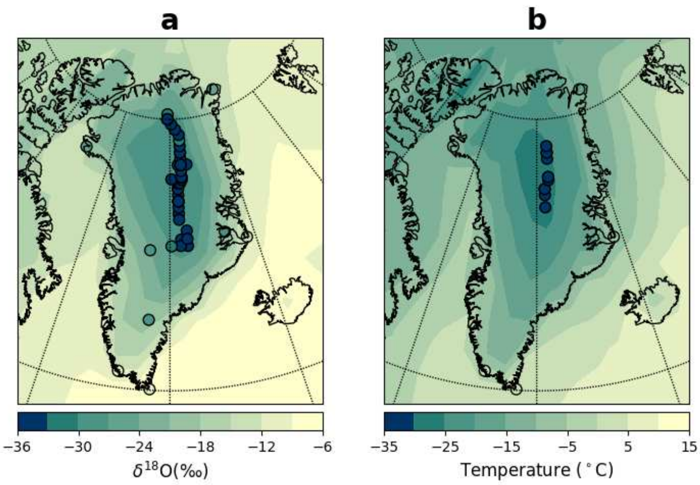

Figure A1. Present-day observations of $\delta^{18}O$ and temperature (Vinther et al., 2010; Sjolte el al., 2011) superimposed onto modelled present-day (1950-2000) values. (a) Annual $\delta^{18}O$ (‰) and (b) annual surface temperatures (°C). Seven transient present-day simulations covering the period 1850-2004 are considered for this analysis. In particular, the shading on each plot shows the mean of these seven present-day simulations for the period 1950-2000.

Appendix B. Modelled uncertainity on $\delta^{18}O$

Figure B.1 shows the simulated annual to decadal variability of annual mean $\delta^{18}O_p$ for a low, medium and high sea ice forcing. $\delta^{18}O_p$ variability is larger near the coast at both annual and decadal time scales (figure B.1). For the sea ice forcing ensemble, at all ice core sites, decadal isotope variability (ranging from standard deviations of 0.36‰ up to 0.62‰ depending on the site) is lower relative to the annual variability (ranging from standard deviations of 0.88‰ up to 1.6‰ depending on the site) (table B.1).

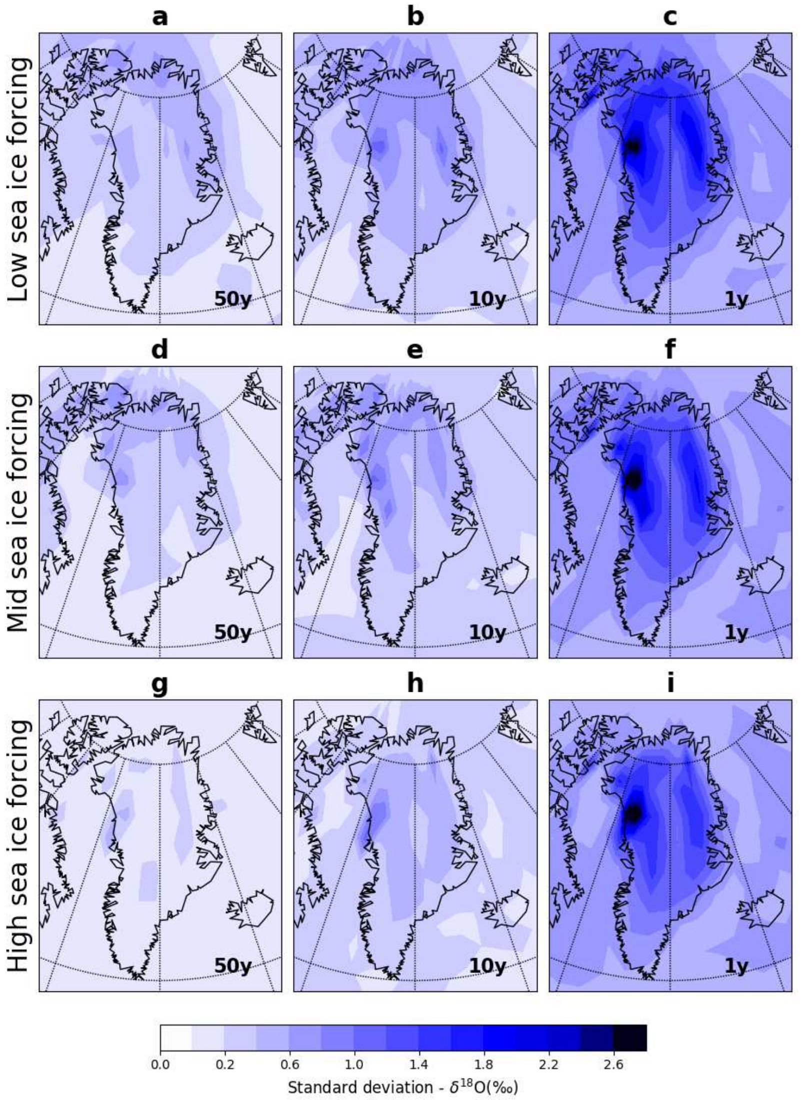

Figure B1. Variability of annual mean $\delta^{18}O_p$ for a low (a-c), medium (d-f) and high (g-i) sea ice forcing, at 50-year average (a, d, g), decadal (b, e, h) and annual (c, f, i) time scales. In particular, the shading in each plot shows the standard deviation between sea ice retreat experiments with a low (between 7% and 19%), medium (between 21% and 65%) and high (between 72% and 100%) winter sea ice loss compared to the PI simulation.

Table B1. Modelled variability of annual mean $\delta^{18}O_p$ at seven ice cores sites at 50-year average, decadal and annual time scales. We list standard deviations (‰) for the sea ice retreat experiments ensemble and a present-day scenario. For the present-day scenario, the standard deviation between seven present-day experiments covering the period 1850-2000 is presented.

	Sea ice forcing ensemble			**Present-day forcing scenario**		
	Standard deviation (‰)			**Standard deviation (‰)**		
Ice core sites	**50-year average**	**Decadal**	**Annual**	**50-year average**	**Decadal**	**Annual**
NEEM	0.24	0.47	1.3	0.22	0.50	1.4
NGRIP	0.24	0.45	1.3	0.19	0.46	1.3
GRIP	0.23	0.36	1.0	0.15	0.34	1.0
Renland	0.28	0.45	1.1	0.33	0.51	1.3
Camp Century	0.35	0.62	1.6	0.30	0.65	1.7
DYE3	0.19	0.37	0.88	0.19	0.36	1.0
GISP2	0.23	0.37	1.1	0.17	0.36	1.1

To complement this model uncertainty analysis on annual mean $\delta^{18}O_p$ values, the standard deviation of 50-year averages are also estimated as this is the time-window used to report all isotope averages in this study. Figure B.1 shows the modelled variability of 50-year averages for a low, medium and high sea ice forcing. For the sea ice forcing ensemble, the standard deviation at this 50-year time scale does not exceed (1) 0.19‰ at DYE3, (2) 0.23‰ at GRIP and GISP2, (3) 0.24‰ at NEEM and NGRIP, (4) 0.28‰ at Renland and, (5) 0.35‰ at Camp Century (table B.1).

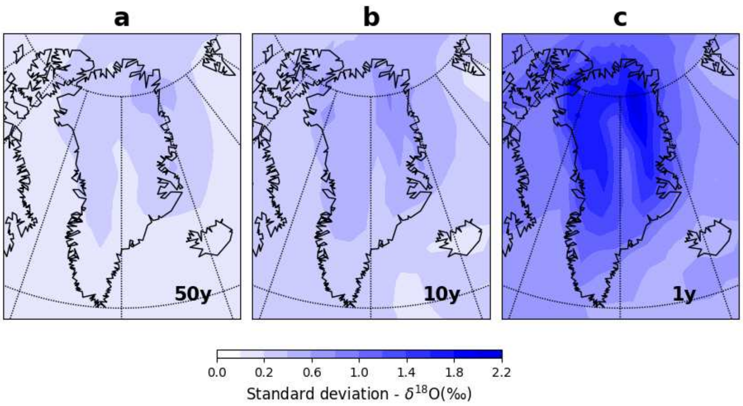

Figure B2. Variability of annual mean $\delta^{18}O_p$ for a present-day scenario at (a) 50-year average, (b) decadal and (c) annual time scales. In particular, the shading in each plot shows the standard deviation between seven present-day experiments covering the period 1850-2000.

For comparison, we also calculated the variability of annual mean $\delta^{18}O_p$ for a present-day scenario at annual, decadal and 50-year average time scales (figure B.2). At all ice core sites, the simulated annual, decadal and 50-year average variability of $\delta^{18}O_p$ for the present-day forcing scenario is very similar relative to the sea ice forcing ensemble (table B.1).

Appendix C. Annual deuterium excess changes

Deuterium excess (hereafter d-excess) has been previously used as a proxy for source area conditions (e.g. Masson-Delmotte et al., 2005; Steffensen et al., 2008). Figure C.1 shows results from the selected 125 ka simulations compared with d-excess data compiled by Landais et al. (2016). We obtain similar values of RMSE for d-excess for the 125ka control simulation (1.1‰), WSIR-7 (1.0‰) and WSIR-35 (1.1‰). The experiment WSIR-7 has the lowest ("best") RMSE (1.0‰), whereas the WSIR-94 experiment shows the highest RMSE (3.4‰). The modelled d-excess results should however be interpreted with caution. The representation of micro-scale cloud physics in HadCM3 does not have a discernible impact on first order $\delta^{18}O$ or δD, but does permit for some tuning of the d-excess (e.g. Tindall et al., 2009; Schmidt et al., 2007; Werner et al., 2011). Better knowledge and improved model representation of micro-scale cloud physics could permit a more insightful analysis of the d-excess data (Landais et al., 2016).

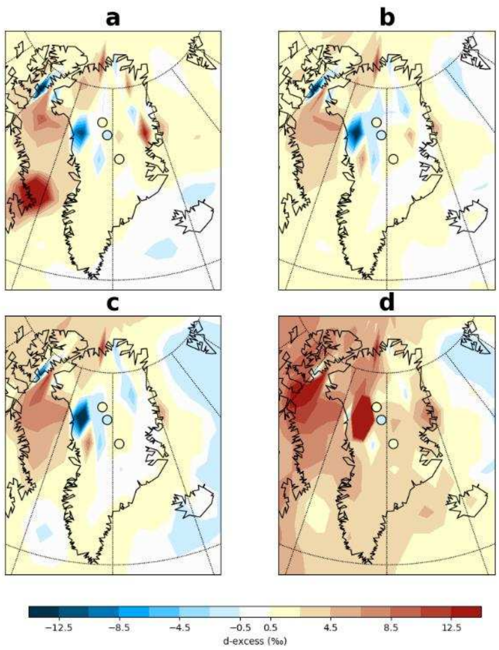

<u>Figure C1.</u> The d-excess data compiled by Landais et al. (2016) superimposed onto modelled annual d-excess anomalies relative to the PI simulation for: (a) 125ka control (RMSE = 1.1‰), (b) WSIR-7 (RMSE = 1.0‰), (c) WSIR-35 (RMSE = 1.1‰) and (d) WSIR-94 (RMSE = 3.4‰).